Journal Pre-proofs

An artificial neural network model for predicting frictional pressure drop in micro-pin fin heat sink

Haeun Lee, Minsoo Kang, Ki Wook Jung, Chirag R. Kharangate, Sael Lee, Madhusudan Iyengar, Chris Malone, Mehdi Asheghi, Kenneth E. Goodson, Hyoungsoon Lee

An artificial neural network model for predicting frictional pressure drop in micro-pin fin heat sink

Haeun Lee[a,b,1], Minsoo Kang[a,b,1], Ki Wook Jung[c], Chirag R. Kharangate[d], Sael Lee[e],

Madhusudan Iyengar[f], Chris Malone[f], Mehdi Asheghi[c], Kenneth E. Goodson[c], Hyoungsoon Lee[a,b,*]

[a]School of Mechanical Engineering, Chung-Ang University, Seoul, 06974, South Korea

[b]Department of Intelligent Energy and Industry, Chung-Ang University, Seoul, 06974, South Korea

[c]Department of Mechanical Engineering, Stanford University, Stanford, CA, 94305, USA

[d]Mechanical and Aerospace Engineering Department, Case Western Reserve University, Cleveland, OH, 44106, USA

[e]Department of Software and Computer Engineering, Department of Artificial Intelligence, Ajou University, Suwon, 16499, South Korea

[f]Google LLC, Mountain View, CA 94043, USA

Abstract: This study is part of two studies conducted for developing artificial neural-network-based tools for predicting the thermal and hydraulic performance of micro-pin fin heat sinks used for high-heat-flux electronic devices. The thermal design of high-heat-flux electronics requires a strong understanding of both pressure drop and heat transfer coefficient. Increasing the pressure drop in a cooling system significantly increases the required pumping power and decreases the system energy efficiency, in addition to considerably increasing temperature nonuniformity and causing reliability issues. Micro-pin fin heat sinks can help in the thermal management of high-heat-flux electronic systems owing to their effective heat transfer characteristics, namely, a large surface area and passage flow turbulence generation, and the requirement of lower pumping power compared with the microchannel heat sink. Studies conducted over the past decade have revealed that the thermal and hydraulic performance of micro-pin fin heat sinks are highly dependent on their geometric and operational parameters. However, a universal approach to predicting the frictional pressure drop, which influences the amount of power required, in pin fin arrays for various operating conditions and geometric shapes has not been developed so far. In this study, a trained artificial neural network (ANN) was used to develop a universal model for predicting the friction factor of micro-pin fin arrays. The friction factor correlation was predicted from 1,651 experimentally determined friction factor data points obtained from 22 studies. The relationship between a wide range of geometric and operating conditions and the hydraulic performance was investigated for accurately training the ANN. Furthermore, the universal model was analyzed by

comparing values predicted by it with values obtained in other experimental studies. The model was found to show superior performance compared with other regression-method-based correlations.

---

* Author to whom correspondence should be addressed: Tel. +82-2-820-5993; E-mail: *leeh@cau.ac.kr*; Website: *http://atsla.cau.ac.kr*
[1] These authors contributed equally to this work.

Nomenclature

A_f	surface area of pin fin, m^2
A_{min}	minimal transverse area of pin fin array, m^2
C_p	specific heat, kJ/kg °C
D_f	hydraulic diameter of pin fin, m
D_w	transverse diameter of pin fin, m
D_L	longitudinal diameter of pin fin, m
f	friction factor
h	heat transfer coefficient, W/m^2 °C
HDR	height-diameter ratio
H_f	pin fin height, m
J	Colburn j-factor
k	thermal conductivity, W/m °C
L	total length of channel, m
$\dot{m}$	mass flow rate, kg/s
N_{tot}	total number of pin fins
N_L	total number of micro-pin fin rows
Nu	Nusselt number
P	wetted perimeter of pin fin, m
Pr	Prandtl number
ΔP	pressure drop, kPa
q''	heat flux, W/m^2
Q	volumetric flow rate, m^3/s
R	coefficient of determination
Re	Reynolds number
S_D	diagonal spacing, m
S_L	longitudinal spacing, m
S_T	transverse spacing, m
T_b	micro-pin fin base temperature, °C
T_f	fluid temperature, °C
u_{max}	maximum fluid velocity, m/s
W	total width of channel, m

Greek symbols

ρ	density of fluid, kg/m^3
η_f	fin efficiency

μ	dynamic viscosity of fluid, kg/m s
θ	percentage of data points predicted within $\pm 30\%$
ξ	percentage of data points predicted within $\pm 50\%$

Subscripts

avg	average
b	base
exp	experiment
eff	effective
f	fluid
h	heater
min	minimum
max	maximum
pred	prediction
tot	total

1. Introduction

The development of micro-electro-mechanical systems (MEMS) has facilitated the development of thermal management techniques for the adequate cooling of high-heat-dissipation systems such as computer data centers, avionics systems, electric vehicles, directed-energy lasers, and military microwave systems. Examples of typical micromachined techniques are the use of microchannels [1,2], spray cooling [3], jet impingement [4], and manifold microchannels [5] for active cooling, and the use of heat pipes [6,7] and vapor chambers [8] for passive cooling. Over the past few years, 3D circuit architectures have enabled the development of high-density transistors for high-performance computing by facilitating the integration of memories, RF devices, optoelectronic devices, and MEMS on a single chip. However, this is often thermally limited due to the increased heat density per unit area and volume, and therefore, there is a need for more compact thermal management solutions with minimal energy consumption [9].

Minimizing the pressure drop is an important requirement in the thermal management of high-heat-flux electronic systems. Increasing pressure drop is undesirable in electronic systems because an appreciable pressure drop significantly increases the required pumping power, and the corresponding increase in power consumption compromises the energy efficiency of the entire system. Moreover, drastic pressure changes can severely degrade the reliability of electronic devices. In particular, a large pressure drop can adversely affect the reliability of high-heat-flux liquid cooling systems since temperature nonuniformity is exacerbated during the phase change

process. Therefore, accurately predicting both pressure drop and heat transfer coefficient are of paramount importance in the thermal design of electronic systems.

Over the past few decades, microchannel heat sinks have greatly increased in popularity for the thermal management of many thermally limited electronic systems, including 3D stack chips, owing to their ease of fabrication, compactness, minimal coolant usage, and outstanding heat transfer coefficients. However, the requirement of a small microchannel height for avoiding electrical delay in 3D stacks results in an extreme pressure drop, leading to low energy efficiency [10,11]. Consequently, microscale pin fins have become indispensable elements for chips fabricated by the 3D staking method, and considerable research has been conducted on optimizing cooling fluids and the geometric shape and arrangement of microscale pin fins for increasing their thermal and hydraulic characteristics [12-43,45,47]. Kosar and Peles [12-14] studied hydrodynamic characteristics of micro-pin fin arrays in both staggered and inline configurations for pin heights (H_f) of 100–243 μm and pin fin diameters (D_f) of 35–100 μm by considering flows of deionized water with Reynolds numbers between 3 and 272. They experimentally found that densely packed pin fins were more effective for cooling for high-Reynolds-number flows, while sparse pin fins were more suited to low-Reynolds-number flows. Prasher *et al*. [15] performed an experimental study with a silicon-based micro-pin fin array in staggered configurations for the D_f range 55–135 μm and for height-to-diameter ratios (*HDR*) of 1.3–2.5. They considered flows of water and circular- and square-shaped pin fins and compared the results in terms of a thermal performance parameter representing the heat transfer per unit of pumping power. Qu and colleagues [16,17] studied single- and two-phase convective heat transfers in staggered copper micro-pin fin arrays for D_f and H_f in the ranges 180–200 μm and 670–683 μm, respectively. They developed a friction factor and heat transfer correlations on the basis of experimental data. However, the correlations were limited for use in various pin fin arrays because of the absence of geometric terms. Tullius *et al*. [18] optimized micro-pin fin parameters such as fin geometry, fin-to-channel height ratio, fin spacing, and fin material for water as the working fluid. They showed that decreasing the fin width and spacing resulted in the Nusselt number increasing with the pressure drop. Furthermore, the use of elliptic and circular fin shapes minimized the pressure drop and remarkably improved the heat transfer performance. Wan and Joshi [19] focused on square-shaped micro-pin fins and compared their hydraulic and thermal performance with those of circular micro-pin fins in terms of the friction factor and Colburn j-factor. Their results showed that circular pin fins exhibited better performance for given pumping power. Kharangate *et al*. [20] investigated heat transfer and pressure drop characteristics of micro-pin fin arrays by using deionized single-phase water with D_f = 46.5 μm and H_f = 110 μm. They proposed correlations for the Nusselt number and friction factor on the basis of experiments and emphasized the necessity for developing correlations that were valid for a broad range of pin fin geometries, flow conditions,

and working fluids. However, the proposed correlations have limitations for use in diverse geometric models because of the lack of geometric terms. Kong *et al*. [21] studied single-phase heat transfer and pressure drop characteristics of embedded silicon micro-pin fin arrays for the D_f range 45–100 μm and for $H_f \cong 200$ μm by using the dielectric fluid R245fa as the working fluid. They showed the influence of *Re* on the Nusselt number and friction factor based on their results, suggesting that there were limitations in deriving the exact correlation owing to the lack of experimental values for the *Re* range 100–400.

Thus, previously developed correlations have limited applicability since their accuracies are guaranteed only within the geometric and operational ranges for which they were developed. This study is the first part of two studies conducted to develop universal tools based on an artificial neural network for predicting the thermal and hydraulic performance of micro-pin fin heat sinks with various geometries for various operational ranges, to overcome the limitations of conventional regression models. We first aimed to develop a predictive tool for predicting the pressure drop in micro-pin fin arrays. We created a consolidated pressure drop database from previous relevant micro-pin fin experimental studies, sufficient to cover a wide range of operating conditions and geometric characteristics. Subsequently, a multilayer perceptron (MLP), which is a type of artificial neural network (ANN), was adopted to predict the Fanning friction factor of micro-pin fin arrays. Compared with conventional regression models, MLPs can be used to model more complex relations between data and thereby achieve higher accuracy in many prediction problems. The friction factor predicted by the MLP was analyzed and compared with the prediction accuracies of both previously proposed models and a new regression model developed in the present study.

2. Methods

2.1 Constructed database from relevant studies

We collected experimental data points for frictional pressure drop in micro-pin fin heat sinks from literature published in the last two decades. The consolidated database amassed from 22 sources consisted of 1,651 frictional pressure drop data points, as summarized in **Table 1,** and Fanning friction factor with respect to Reynolds number in the amassed database, as shown in **Figure 1**. Some of the studies are purposely excluded when they included i) micro-pin fin with a tip clearance, ii) presence of non-condensables, iii) unclear information in geometrical or operational conditions, or iv) parameters that do not fit into the new correlation to be developed. We first intentionally excluded all the data points with a tip clearance between pin fins and the
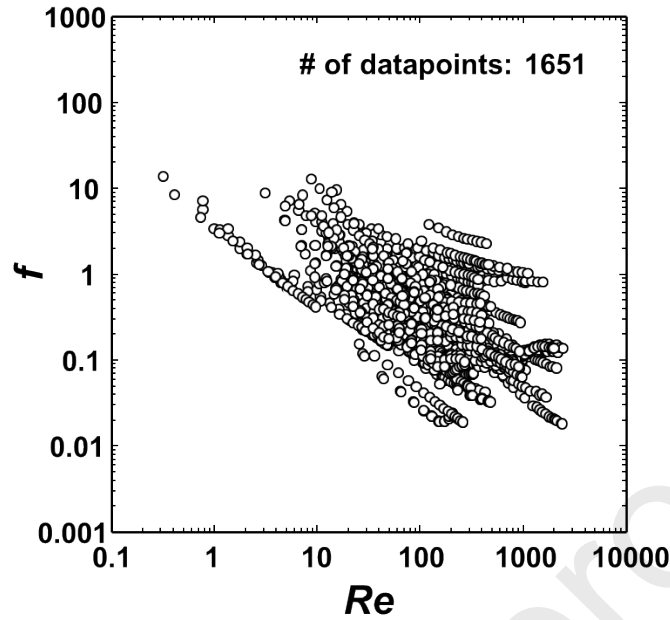
Figure 1 A 1,651-point consolidated database for Fanning friction factor in micro-pin fin heat sinks from 22 sources.

top cover of the channel (Moores and Joshi [22] and Mei *et al.* [23]) or working fluid that included any non-condensable gases (Chyu *et al.* [24] and Jeng *et al.* [25]) due to its complexity of fluid flow and difference in flow characteristics. Irregular shapes of pin fins such as Piranha pin, hydrofoil, and oblique fin (Woodcock *et al.*[26], Sarvey *et al.* [27], Lee *et al.*[28]) were also excluded due to the difficulty obtaining accurate geometrical dimensions, such as the hydraulic diameter and minimum fin spacing. Some studies were also excluded due to insufficient geometry information (Liu *et al.*[29]) or $(S_L\text{-}D_f)/D_f \leq 0$ (Brunschwiler [30]), since they could not be predicted using existing correlations. In addition, some data of Brunswhiller [30] originate from heat transfer structures with pearl chain shapes; because the respective D_f cannot be defined, these data were excluded. Regarding the results of Rasouli [40] and Kosar&Peles [14], only the visible data could be extracted for the analysis. The consolidated data includes geometrical information of hydraulic diameter (D_f), pin fin height (H), the transverse pitch of the fins (S_T), the longitudinal pitch of the fins (S_L), shapes of pin fins, and flow configurations with the detailed operating conditions of mass flow rate ($\dot{m}$), inlet and outlet fluid temperature (T_{in}, T_{out}), heat flux (q''), Reynolds number (Re), pressure drop (ΔP), and corresponding Fanning friction factor (f). The D_f, Re, and f were determined using the following definitions:

$$D_f = \frac{4A_f}{P},\tag{1}$$

$$Re = \frac{\rho u_{max} D_f}{\mu},\tag{2}$$

$$f = \frac{\Delta P}{2\rho u_{max}^2 N_L} . \tag{3}$$
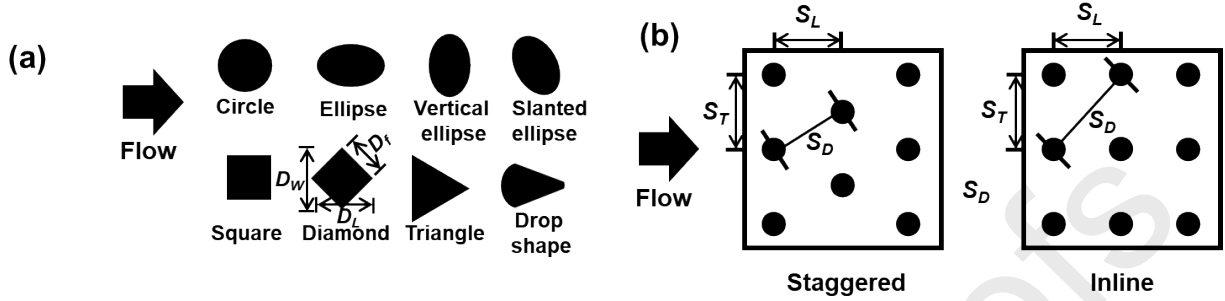
Figure 2 Geometrical configurations of (a) pin fin shapes and (b) flow types.
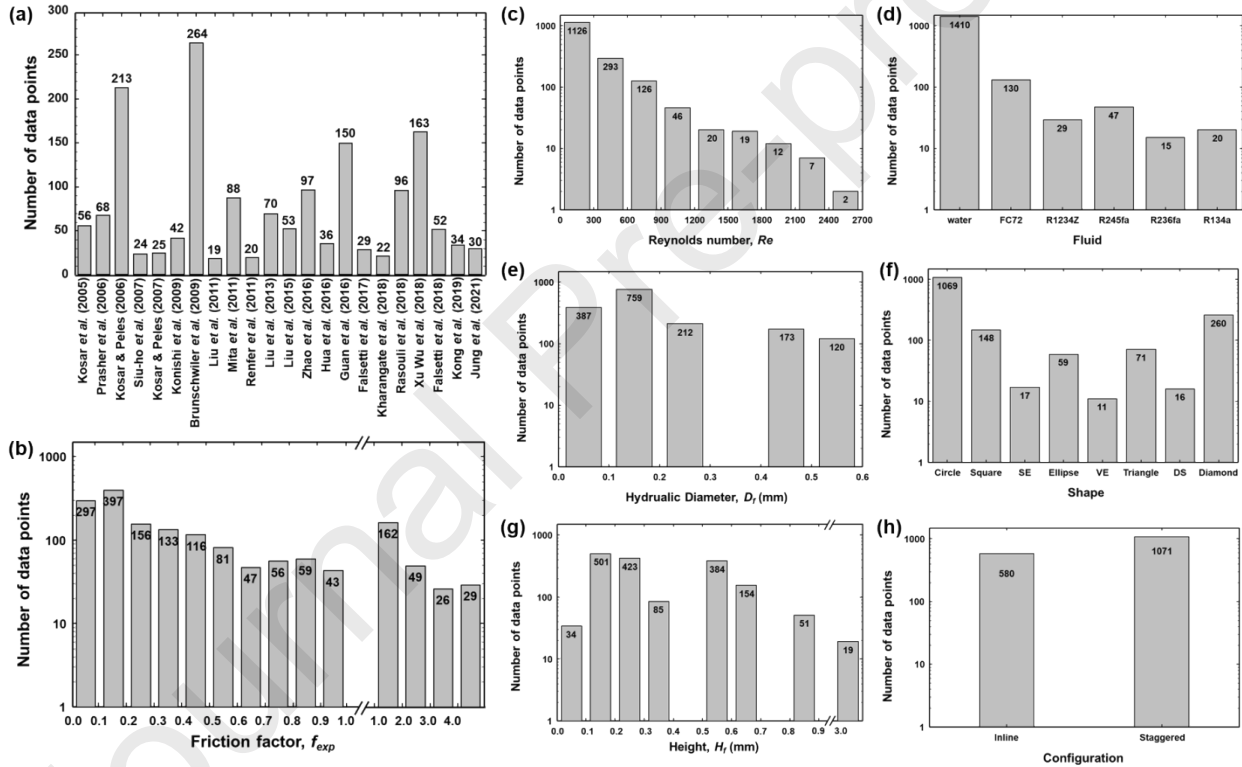
Figure 3 Distribution of data points (a) sources, (b) friction factor, (c) *Re*, and (d) working fluids, and geometric parameters of (e) pin fin diameter, (f) pin fin shape, (g) pin fin height, and (h) fin configuration.

A_f and P are fin cross-sectional area and perimeter, respectively. u_{max} is the maximum fluid velocity, which can be determined as

Inline:
$$u_{max} = \frac{S_T}{S_T - D_f} u_{in}, \tag{4-1}$$

Table 1 Summary of frictional friction factor studies for micro-pin fins included in the consolidated database.

| Author	Shape	Config	Fluid	f	Re	D_f [mm]	H_f [mm]	q'' [W/cm²]	Operating condition	Total data points	Included data points	Remark
Koşar et al. [12]	C, D	ST IN	Water	0.27 - 8.25	5 – 100	0.05 - 0.1	0.1 - 0.2	Adiabatic	$\dot{m}$ = 0.47 – 3.9 g/min T_{in} = 22 ºC	56	56	Converting from Darcy f to fanning f
Prasher et al. [15]	C, S	ST	Water	0.09 - 1.14	40 – 1000	0.055 - 0.15	0.2 – 0.31	Adiabatic	$\dot{m}$ = 9.98 – 199.6 g/min ΔP = 0 – 250 kPa T_{in} = 50 ºC	68	68	
Kosar & Peles [14]	C, D	ST IN	Water	0.08 - 12.75	3.1 – 271.8	0.035 - 0.1	0.243	Adiabatic		213	213	Converting from Darcy f to fanning f
Siu-ho et al. [16]	S	ST	Water	0.07 - 0.16	120 – 700	0.2	0.67	50 – 100	T_{in} = 25 ºC $\dot{m}$ = 83.4 – 644.2 g/min	24	24	
Kosar & Peles [13]	C	ST	Water	0.18 - 2.03	14 – 250	0.1	0.1 - 0.243	Adiabatic	$\dot{m}$ = 0.6 – 9 g/min	59	25	Excluding some uncertain data points
Konishi et al. [17]	S	ST	Water	0.4 - 0.83	35 – 260	0.2	0.67	Adiabatic	T_{in} = 21 – 80 ºC $\dot{m}$ = 36.6 – 90.6 g/min	42	42	
Brunschwiler et al. [30]	C, DS	ST IN	Water	0.02 - 111.57	<1000	0.025 - 0.1	0.1 - 0.2	Adiabatic	$\dot{m}$ = 50 – 210 g/min T_{in} = 25 ºC	307	264	Pearl chain shape and S_L = D_F are excluded
Liu et al. [31]	D	ST	Water	0.13 - 0.59	80 – 700	0.63 - 0.79	3.0	50 – 350	Q = 5.693 – 57.221 L/h T_{in} = 30 – 70 ºC	19	19	Converting Darcy to fanning
Mita et al. [32]	C	ST	Water	0.12 - 0.4	25 – 800	0.18	0.683	Adiabatic	T_{in} = 23 – 80 ºC $\dot{m}$ = 34.32 – 318.9 g/min	88	88	Converting Darcy to fanning
Renfer et al. [33]	C	IN	Water	0.07 - 0.58	14.5 – 270.4	0.1	0.2	Adiabatic		20	20	Calculating f using pressure drop
Liu et al. [34]	C	ST IN	Water	0.18 - 1.1	8.6 – 396.5	0.5	0.5	Adiabatic		70	70	Converting from W/4L to N_L
Liu et al. [35]	C, E, D	ST	Water	0.06 - 0.85	108.6 – 970.2	0.4 - 0.56	0.5	Adiabatic		53	53	Converting Darcy to fanning
Zhao et al. [36]	C, S, D, E, T	ST	Water	0.02 - 1.39	100 – 2500	0.28 - 0.72	0.5	Adiabatic		97	97	Converting Darcy to fanning
Hua et al. [37]	C	ST	Water	0.04 - 1.76	70 – 1700	0.4	0.3	Adiabatic	$\dot{m}$ = 0 – 199.6 g/min ΔP = 0 ~ 40 kPa	36	36	Only new data included. f from pressure drop & Q
Guan et al. [38]	C, D, T	ST	Water	0.18 - 1.21	47 – 922.8	0.28 - 0.72	0.5	*50 – 150 W		150	150	Calculating f using pressure drop *Heated area not specified
Falsetti et al. [39]	C	IN	R1234ze (E)	0.09 - 0.18	230 – 2500	0.05	0.1	20 – 44	T_{out} = 25, 30, 35 ºC	29	29	Converting from W/L to N_L
Kharangate et al. [20]	C	ST	Water	0.2 -0.5	23 - 135	0.047	0.11	24 – 141.4	$\dot{m}$ = 15.1 – 64.1 g/min P_{in} = 144.4 ~ 340.1 kPa P_{out} = 132.0 – 201.0 kPa T_{in} = 25 ºC, T_{out} = 31.5 – 84.3ºC	22	22	
Rasouli et al. [40]	D	ST	FC-72	0.69 - 5.33	15 - 1500	0.18 - 0.2	0.396 – 0.845	Adiabatic		Not specified	96	Exact number is not specified
Xu_Wu et al. [41]	C, S, D, E, SE, VE	ST IL	Water	0.27 - 3.96	40 – 1000	0.1 - 0.15	0.11	Adiabatic	$\dot{m}$ = 3 – 42 g/min T_{in} > 30 ºC	163	163	Converting from W/L to N_L
Falsetti et al. [42]	C	IL	R236fa, R134a, R245fa	0.1 - 0.31	230 – 2500	0.05	0.1	20 – 44	T_{out} = 25 ºC	52	52	Converting from W/L to N_L and A_{ch} to A_{min}
Kong et al. [21]	C	ST	R245fa	0.03 - 0.51	35 – 500	0.045 - 0.1	0.2 – 0.208	2.5 – 48.7	T_{in} = 22.2 – 25.3 ºC $\dot{m}$ = 14.7 – 181.6 g/min	30	30	
Jung et al. [43]	C	ST	FC-72	0.08 - 0.18	81 – 182	0.038	0.091	0 – 60	Q = 70 – 140 g/min	34	34	

Staggered:
$$u_{max} = \max\left(\frac{S_T}{S_T - D_f} u_{in}, \frac{S_T}{2\left(S_D - D_f\right)} u_{in} \right), \tag{4-2}$$

where u_{in} is the inlet fluid velocity of the channel. This is because, in the case of the inline flow configuration, the transversal spacing determines the minimal area through which the flow flows; in the case of the staggered flow configuration, the minimal area is determined based on the smallest transversal or diagonal spacing. Here, we include two more parameters, D_W and D_L, which represent the projected and longitudinal diameter of pin fin along the flow direction, to distinguish cases of the same hydraulic diameter but different in pressure drops, such as ellipse and slant. The detailed pin fin shapes (a) and fin configurations (b), used in the consolidated database, are illustrated in **Figure 2**.

Figure 3 shows the distribution of data according to geometries and operating conditions. **Figure 3**(a) shows the number of data points extracted from each source. **Figure 3**(b) to (h) show number of data points with respect to the Fanning friction factor, Reynolds number, type of

working fluid, hydraulic diameter, shape of pin fin, fin height, and fin configuration. In all, the consolidated database includes 1,651 data points, which covers the following ranges:

- Pin fin shape: Circle (C), Square (S), Diamond (D), Ellipse (E), Triangle (T), Dropped shape (DS), Slant ellipse (SE), Vertical ellipse (VE)
- Configuration (Config): Staggered (ST), Inline (IL)
- Working fluid: Water, FC72, R1234ze (E), R134a, R236fa, R245fa
- Hydraulic diameter (D_f): 30–560 μm
- Height of channel and pin fin (H_f): 91–3,000 μm
- Spacing of Length (S_L): 50–1,200 μm
- Spacing of Transverse (S_T): 50–1,130 μm
- Channel length (L): 0.51–4 cm
- Reynolds number (Re): 0–2,500

2.2 Selection of input parameters

We first compared the Pearson correlation coefficient (PCC) of the Fanning friction factor to evaluate the linear association between each parameter and the Fanning friction factor. PCC is a statistic that measures a linear correlation between two variables, and it is expressed as follows:

$$R_{xy} = \frac{\sum_{i}^{n}(X_i - \bar{X})(Y_i - \bar{Y})}{\sqrt{\sum_{i}^{n}(X_i - \bar{X})^2}\sqrt{\sum_{i}^{n}(Y_i - \bar{Y})^2}}. \tag{5}$$

R has a value between +1 and −1 where +1, 0, and -1 represent total positive linear correlation, no linear correlation, and total negative linear correlation, respectively. **Figure 4** shows the PCCs of the Fanning friction factor based on micro-pin fin geometrical parameters and Reynolds number. Here, we evaluated the R-value separately based on Re ~100, since several micro-pin fin studies claimed that there are changes of flow characteristics at Re ~100 [15,19]. As shown in **Figure 4**, the effects of geometric parameters on the friction factor vary depending on the range of Re. The Re dominates the friction factor, and the effects of geometrical parameters are relatively small compared to the range of low Re. However, their effects increase significantly for the higher Re range (Re>100), while Re is still the most dominant parameter effect on the friction factor. Unlike other geometric parameters, the transverse spacing (S_T) effect is decreased for the higher Re region. It is estimated that the variances of S_T show a relatively small difference in the range Re < 100 and Re > 100, while the variances of all other parameters more than doubles in the same range. This suggests that all the investigated geometric parameters are needed to be considered for predicting the friction factor. Consequently, we selected the input parameters of S_L, S_T, H_f, D_f, D_W, D_L with Re for taking into account the effect of a small number of pin fin rows [44]. All the input parameters were used in a natural logarithmic form to train and test the MLP prediction model. Log

-- 10 --

transformation of input and output parameters is known to improve the stability of the model, especially when the relationship between input parameters and output parameters is close to curvilinear in nature [45].
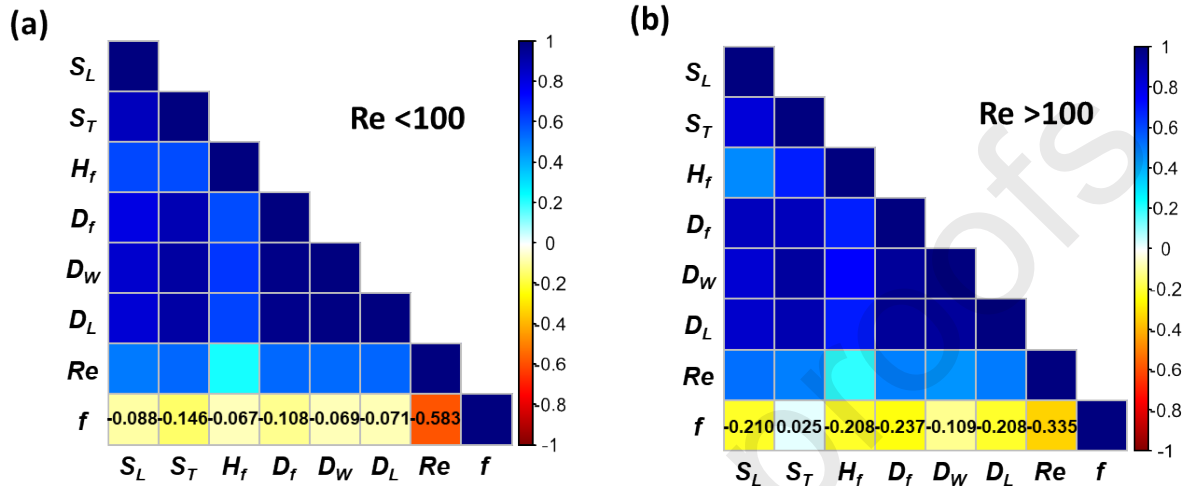

Figure 4 Pearson correlation coefficients of the Fanning friction factor with respect to pin-fin parameters.

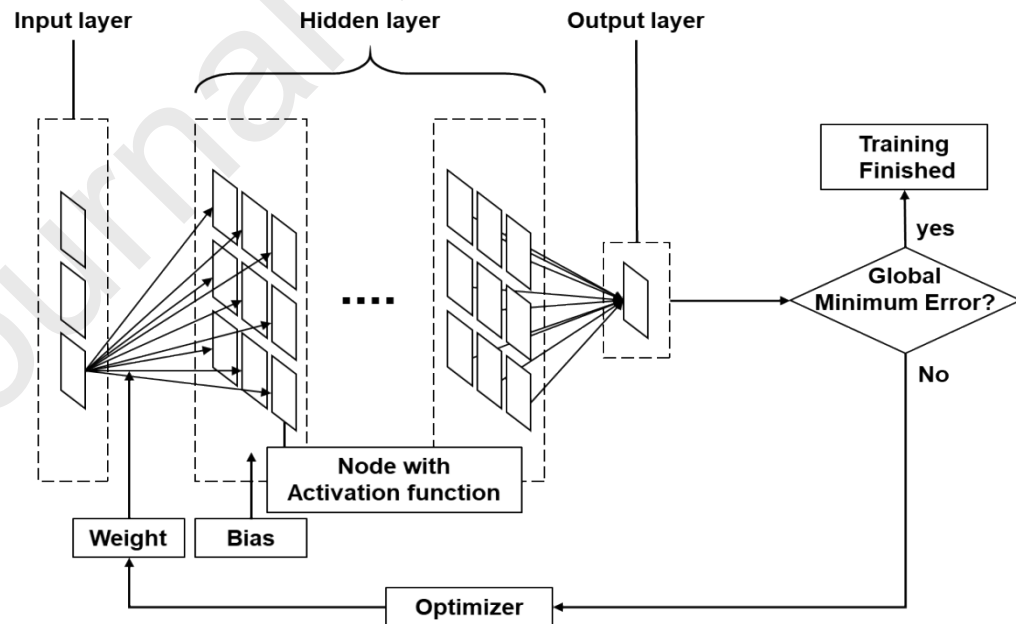## 2.3 Multilayer perceptron neural network

Figure 5 Architecture of a multilayer perceptron

There have been many studies for developing empirical correlations to predict the friction factor in micro-pin fin arrays [15-17,19,20,45,47]. Usually, conventional regression models are used to find relationships between friction factors, but these correlations show poor predictive accuracy in the outranged data of their geometrical or operational conditions. Moreover, conventional regression models are not powerful enough to capture all the geometrical and fluid flow complexities of the micro-pin fin array. Therefore, we adopted a multilayer perceptron (MLP)[48], a type of artificial neural network (ANN) that is widely used to model complex interdependent parameters. Training our MLP model with our carefully constructed dataset allows for a universal prediction of friction factor in micro-pin fin array that aims to cover a wide range of geometrical and operational variations. **Figure 5** shows the structure of our MLP with weights, bias, layers, functions, and optimizer.

Our MLP was trained using Tensorflow (version 1.13.1) and Numpy (version 1.17.0). The two tools enabled us to handle and train the multidimensional matrix arrays based on Python (version 3.6). First, our model minimizes the cost (Y_{pred} - Y_{exp}) with Y_{pred} = $XW + b$. In this case, X is the input parameter of the data, W the weight, and b the bias. In addition, X is a matrix with the size (number of data) $\times$ (number of parameters), and W is a matrix with the size (number of parameters) $\times$ (number of nodes). As the number of nodes increases, the learning accuracy and the fact whether overfitting or underfitting occurs are determined. After adding a bias to the calculated XW matrix value, this value is substituted into the activation function.

The Leaky Rectified Linear Unit (LReLU) [49], which is a modified ReLU [50] function that prevents convergence to zero, was used as an activation function; it can be expressed as follows:

$$f\left(x\right)=\begin{cases} x & \text{for} \quad x \geq 0 \\ 0.2x & \quad\quad\ x < 0 \end{cases}. \tag{6}$$

The weights were initialized with the He method, which works well for PReLU [51] (similar tendency to that of the LReLU), and bias is initialized to zero. The LReLU was used as the activation function in the hidden layer, and the identity function was used in the output layer. The outputs were updated with the widely used Adam optimizer [52] during training; it combines AdaGrad [53] and RMSprop [54]. When the data amount is limited, cross validation improves accuracy and prevents overfitting; for example, the K-fold method is one of the most commonly used methods [55],[56]. The method classifies the data into a training set and a test set; in the next step, the train data are classified into K groups for cross-validation. K-fold cross-validation with K=5 was used to train and validate the data. In addition, the early stopping method, which is also a widely adopted neural network trick, was used to minimize the number of iterations while

preventing overfitting to the training data. This method assesses whether the learning process has converged and is completed. In our model, the patience is set to 1500, which means that if the MAE of the validation set continues to increase 1500 times, the minimum is the point at which the training process is considered complete.

The hyperparameters of MLP—the numbers of hidden layers and nodes per layer—were chosen from different combinations of hidden layers and nodes per layer based on the predictive accuracy of the validation set after training the MLP on the training set. More specifically, the consolidated data were randomly divided into three groups— training (72%), validation (18%), and test (10%)—, and then the predictive accuracies with different numbers of layers and nodes combinations were determined using mean absolute error (MAE) of the validation set. We report our final accuracy using the test dataset. The equation for MAE is as follows:

$$MAE = \frac{1}{n} \sum_{n} \frac{\left| f_{exp} - f_{pred} \right|}{f_{exp}} \times 100 \ (\%).$$

(7)
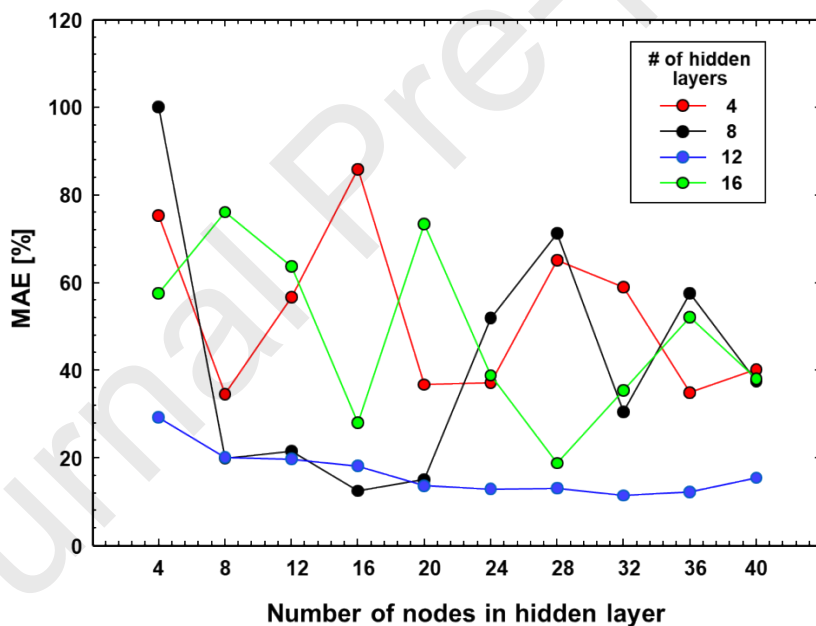
Figure 6 MLP model predicting accuracies with different combinations of numbers of nodes and hidden layers.

Figure 6 shows validation MAEs for different combinations of numbers of hidden layers and nodes per each hidden layer. For this study, the combinations of 12 layers and 28 nodes set is adopted since it shows the low validation MAE of 13.01% while providing a minimum difference between training MAE and validation MAE. The detailed MAE data for each combination can be found in **Table S1** in **Supplementary Information (Appendix A)**.

-- 13 --

3. Results

3.1 Assessment of previous and new regression models

Here, we compare the MAEs with the predictions of existing correlations and our proposed correlation developed from the consolidated database. **Table 2** shows a summary of the existing friction factor correlations of micro-pin fin available in the literature. The proposed correlation was deduced using GRG (generalized reduced gradient) nonlinear regression analysis based on a decent algorithm, aiming to minimize MAE [57,58].

Figure 7 shows comparisons of experimentally determined Fanning friction factors with predictions of (a) the proposed model, and (b-h) existing correlations available in the literature. The proposed regression correlations are separated into two equations, which are divided based on $Re = 100$. The existing correlations are selected as the most relevant and highly cited correlations for the micro-pin fin geometries among the correlations suggested by researchers in the last two decades. Three different parameters, θ, ξ, and MAE, are used to compare the predicting capabilities of each correlation where θ and ξ exhibit the percentage of data points predicted within ±30% and ±50%, respectively.

Table 2 Previous micro-pin fin friction factor correlations.

	Author(s)	Equation	Fluid	Geometry	Operating Condition
1	Present study	$f = 3.704\left(\frac{H_f}{D_f}\right)^{-0.214}\left(\frac{S_L-D_f}{D_f}\right)^{0.349}\left(\frac{S_T-D_f}{D_f}\right)^{-0.870}\left(\frac{D_W}{D_f}\right)^{1.656}\left(\frac{D_L}{D_f}\right)^{2.708} Re^{-0.668}$ for $Re < 100$ $f = 0.270\left(\frac{H_f}{D_f}\right)^{0.620}\left(\frac{S_L-D_f}{D_f}\right)^{0.710}\left(\frac{S_T-D_f}{D_f}\right)^{-0.501}\left(\frac{D_W}{D_f}\right)^{0.050}\left(\frac{D_L}{D_f}\right)^{0.047} Re^{-0.294}$ for $Re > 100$ $f = 1.569\left(\frac{H_f}{D_f}\right)^{0.244}\left(\frac{S_L-D_f}{D_f}\right)^{0.164}\left(\frac{S_T-D_f}{D_f}\right)^{-0.919}\left(\frac{D_W}{D_f}\right)^{1.851}\left(\frac{D_L}{D_f}\right)^{0.367} Re^{-0.539}$ for all Re	Water FC72 R1234ze R134a R236fa R245fa	Staggered & Inlined Circle, Square, Triangle, Ellipse, Diamond, Dropped shape $25\mu m < D_f < 720\mu m$ $H_f = 0.09 – 3$ mm $S_T = 0.05 – 1.1$ mm $S_L = 0.05 – 1.2$ mm	$Re = 0 - 2440$
2	Prasher *et al.* [15]	$f = 169.82\left(\frac{H_f}{D_f}\right)^{-0.640}\left(\frac{S_L-D_f}{D_f}\right)^{-0.258}\left(\frac{S_T-D_f}{D_f}\right)^{0.283} Re^{-1.350}$ for $Re < 100$ $f = 0.295\left(\frac{H_f}{D_f}\right)^{1.249}\left(\frac{S_L-D_f}{D_f}\right)^{-0.700}\left(\frac{S_T-D_f}{D_f}\right)^{-0.360} Re^{-0.100}$ for $Re < 100$	Water	Staggered, Circle, Square $55\ \mu m < D_f < 153\ \mu m$ $1.3 < H_f/D_f < 2.8$ $2 < S_T/D_f < 4$ $2 < S_L/D_f < 4$	$Re = 40 - 1000$ $T_{in} = 50$ °C
3	Siu-ho *et al.* [16]	$f = 5.023 Re^{-0.547}$	Water	Staggered, Square $D_f = 200\ \mu m$ $H_f = 670\ \mu m$ $S_T = S_L = 400\ \mu m$	$Re = 37.9 - 85.8$ $T_{in} = 21$ °C
4	Moores *et al.* [46]	$f = 2.63\left(\frac{H_f}{D_f}\right)^{0.289} Re^{-0.390}$	Water	Staggered, Circle $0.5 < H_f/D_f < 1.1$ $1.3 < S_T/D_f < 1.36$ $1.13 < S_L/D_f < 1.18$	$q'' = 0.016 - 0.24$ W/mm² $Re = 200 - 10,000$ $T_{in} = 27$ °C
5	Konishi *et al.* [17]	$f = 2.621 Re^{-0.350}$	Water	Staggered, Square $D_f = 200\ \mu m$ $1.3 < H/D_f < 2.8$ $2 < S_T/D_f < 4$ $2 < S_L/D_f < 4$	$Re = 0 - 300$
6	Roth *et al.* [47]	$f = 12.919 Re^{-0.923}$	Water	Staggered & inlined, Circle $H_f = 91.1$ & 128.9 μm $S_T = 91.1$ & 129.3 μm $C/D_f = 0.56$ to 0.77	$Re = 9 - 238.4$ $T_{in} = 50$ °C
7	Wan & Joshi [19]	$f = 3.355\left(\frac{H_f}{D_f}\right)^{-0.356}\left(\frac{S_L-D_f}{D_f}\right)^{-0.791}\left(\frac{S_T-D_f}{D_f}\right)^{-0.745} Re^{-0.525}\frac{L}{D_f N_L}$ for $Re < 100$ $f = 0.586\left(\frac{H_f}{D_f}\right)^{-0.051}\left(\frac{S_L-D_f}{D_f}\right)^{-0.175}\left(\frac{S_T-D_f}{D_f}\right)^{-0.249} Re^{-0.552}\frac{L}{D_f N_L}$ for $Re > 100$	Water	Staggered, Square $D_f = 200\ \mu m$ $H_f/D_f = 1.5$ $S_T/D_f = 2$ $S_L/D_f = 2$	$Re = 22 - 357$ $T_{in} = 25$ °C
8	Kharangate *et al.* [20]	$f = 2.5 Re^{-0.520}$	Water	Staggered, Circle $D_f = 46.5\ \mu m$ $H_f/D_f = 2.37$ $S_T/D_f = 2.15$ $S_L/D_f = 2.15$	$q'' = 24.0 - 141.4$ W/cm² $Re = 23 - 135$ $T_{in} = 25$ °C

As shown in **Figure 7**, Prasher [15] and Moores [45] show very low predictions with MAEs of 285.14% and 167.53%, respectively, even though geometric terms are included in the correlations. Moores' correlation [45] exhibited a large MAE since their experimental data included both with and without pin fin tip clearance with relatively high inlet fluid temperature compared to other experimental conditions in the consolidated database. Siu-ho *et al.*[16] and Konishi *et al.* [17] also provided poor predictions for the database, with MAEs of 133.89% and 171.77%, respectively, since both correlations are independent of any geometric terms and their geometric parameter ranges are relatively large compared to the ranges in the database.

Roth *et al.*[47] and Wan & Joshi [19] showed fair predictions, with MAEs of 75.95% and 74.36%. Wan & Joshi [19] presented two correlations based on the boundary ($Re = 100$) speculated as a range of transitions from laminar to turbulent. In the range of $Re > 100$, the MAE value was 62.12%, whereas the prediction was relatively poor, with the MAE of 97.15% in the range of Re <100. Notice that the Kharangate correlation [20] shows the highest accuracy among the previous correlations, evidenced by the MAE, θ, and ξ of 68.43%, 27.14%, and 45.55%, respectively, although it does not contain any geometric terms; mainly because the experimental data used to establish their correlation was distributed in nearly the median of both hydraulic diameter and Re of the consolidated database. The present regression model provides the best prediction accuracy, with an overall MAE of 52.33%. However, despite the low overall MAE, θ and ξ are low with 33.01% and 49.42%. The most data points did not come within 30% of prediction because the predicted data points are slightly underestimated in the low Re range.
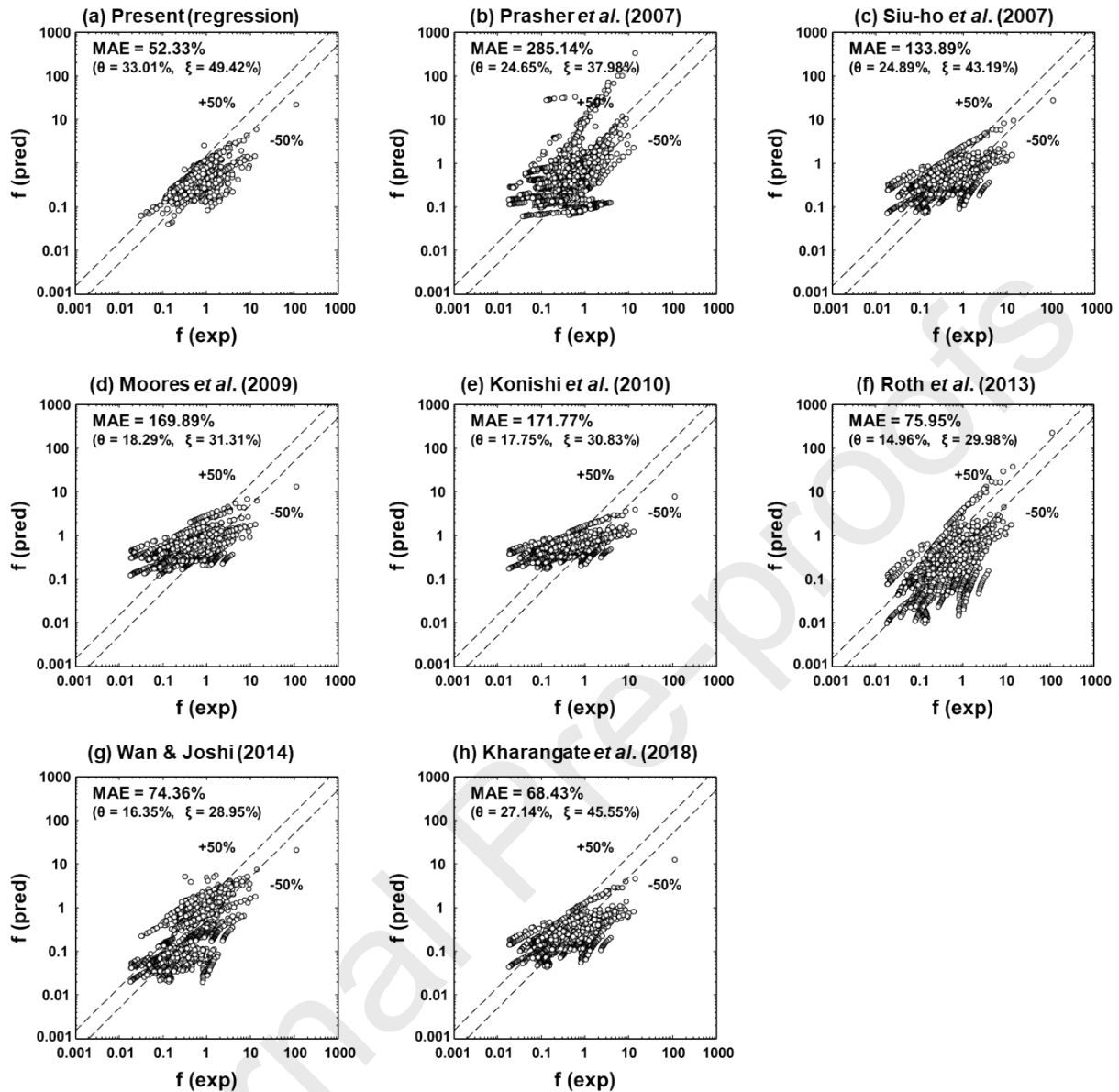
Figure 7 Comparison of experimentally determined Fanning friction factor with predictions of (a) new regression correlation, (b) Prasher *et al.* [15], (c) Siu-ho *et al.* [16], (d) Moores *et al.* [45], (e) Konishi *et al.* [17], (f) Roth *et al.* [47], (g) Wan & Joshi [19], and (h) Kharangate *et al.* [20].
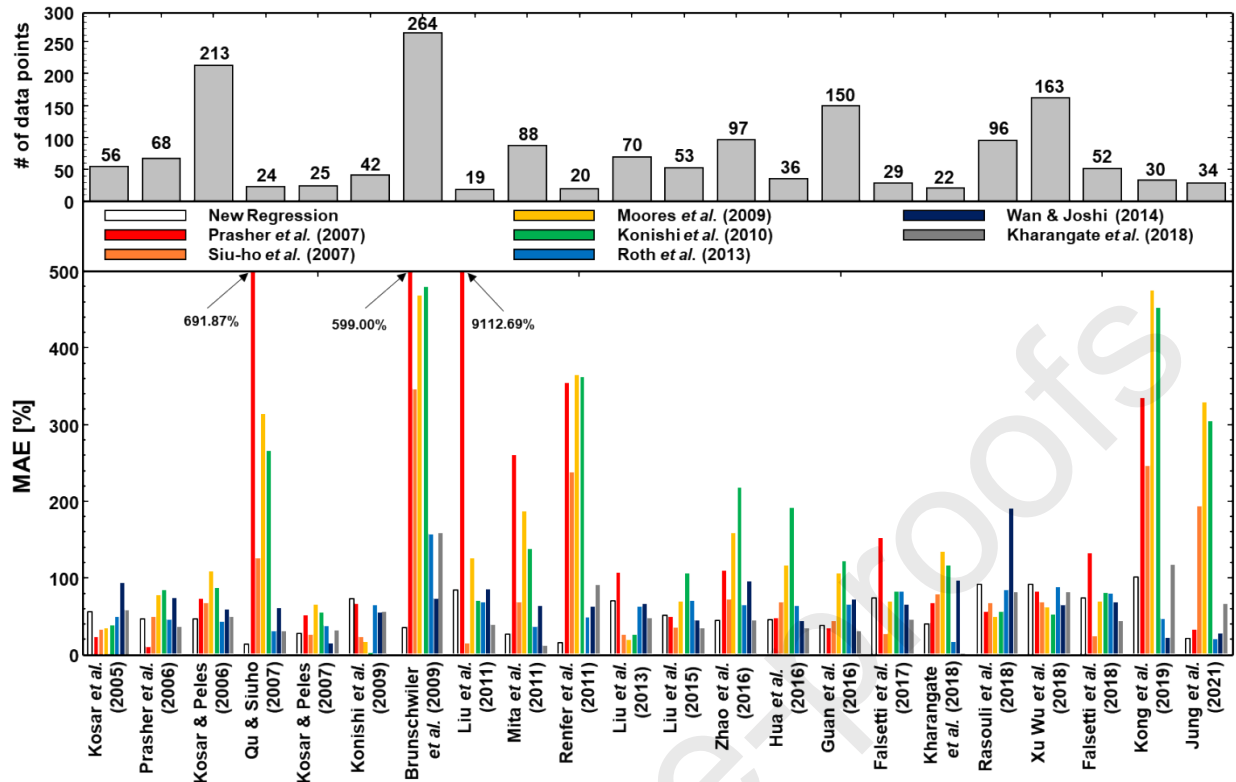
Figure 8 Comparison of individual experimentally-determined friction factor data points with predictions of relevant existing and present correlations.

Figure 8 illustrates the predictions of eight selected relevant correlations and presents a regression correlation against the individual Fanning friction databases from 22 sources. The present regression correlation provides evenly fair predictions, with MAEs < 99.6% for all 22 individual databases. The correlations of Wan & Joshi [19] and Kharangate *et al.* [20] have also shown fair predictions, with a range of MAEs < 191.0% for the individual databases. The Prasher *et al.* [15] correlation has provided fairly reasonable predictions for most individual databases but poor predictions for Siu-Ho *et al.* [16], Brunschwiler *et al.* [30], and Liu *et al.* [31] with MAEs of 691.9%, 599.0%, and 9112.7%, respectively. These low accuracies are mainly based on the large discrepancies in geometric and operational ranges such as high aspect ratio (HDR, H/D$_f$= 5.4–6.7, 3.4) [16,31], and specific low *Re* range (*Re* < 10) [30]. Some correlations show poor predictions for Kong *et al.*'s database [21] with MAEs of 334.9%, 246.7%, 475.3%, and 453.4% for Prasher *et al.* [15], Siu-Ho *et al.* [16], Moores *et al.* [45], and Konishi *et al.* [17], respectively. In comparison, others provide MAEs of 23.3–118.1% since they were tested in the limited Reynolds number range with R245fa as a working fluid.
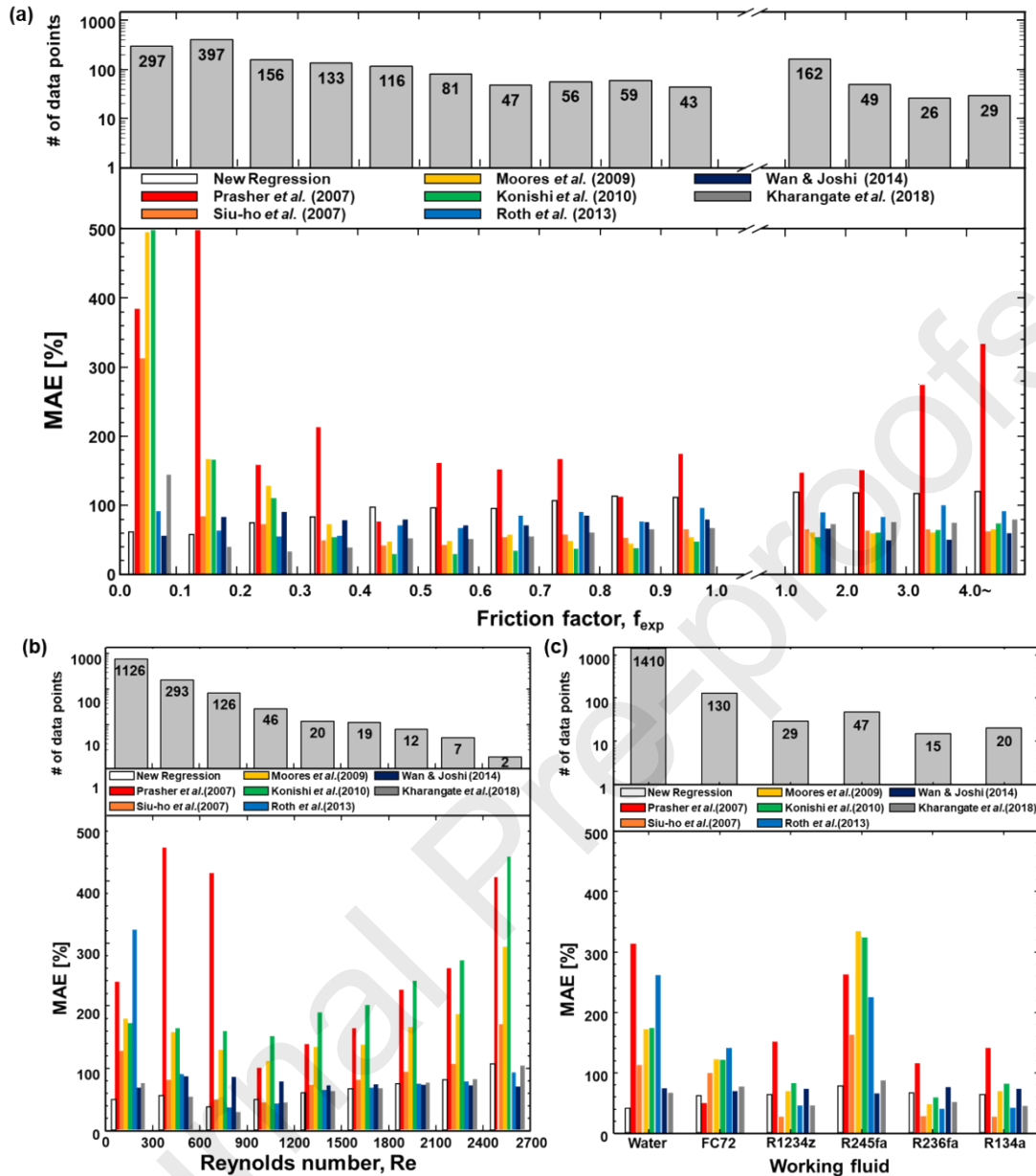
Figure 9 Distribution of MAE in predictions of present regression correlation and selected relevant correlations relatives to (a) friction factor, (b) Reynolds number, and (c) working fluid.

Figure 9 shows the predictions according to the operational conditions of the present regression correlation and the relevant correlations. As shown in **Figure 9**(a), most correlations show high MAEs in the low friction factor range of f = 0–0.1 because some of those low friction factors are from high Re (Re < 2400) while most of the previous correlations were developed in a low Re range (Re < 1000). Moores et $al.$ [45] has developed for a wide Re range of Re = 200–10000 but also provided poor prediction in this f range. In the higher f range (f > 3.0), most correlations show relatively large MAEs, while better predictions are made in the moderate f

-- 18 --
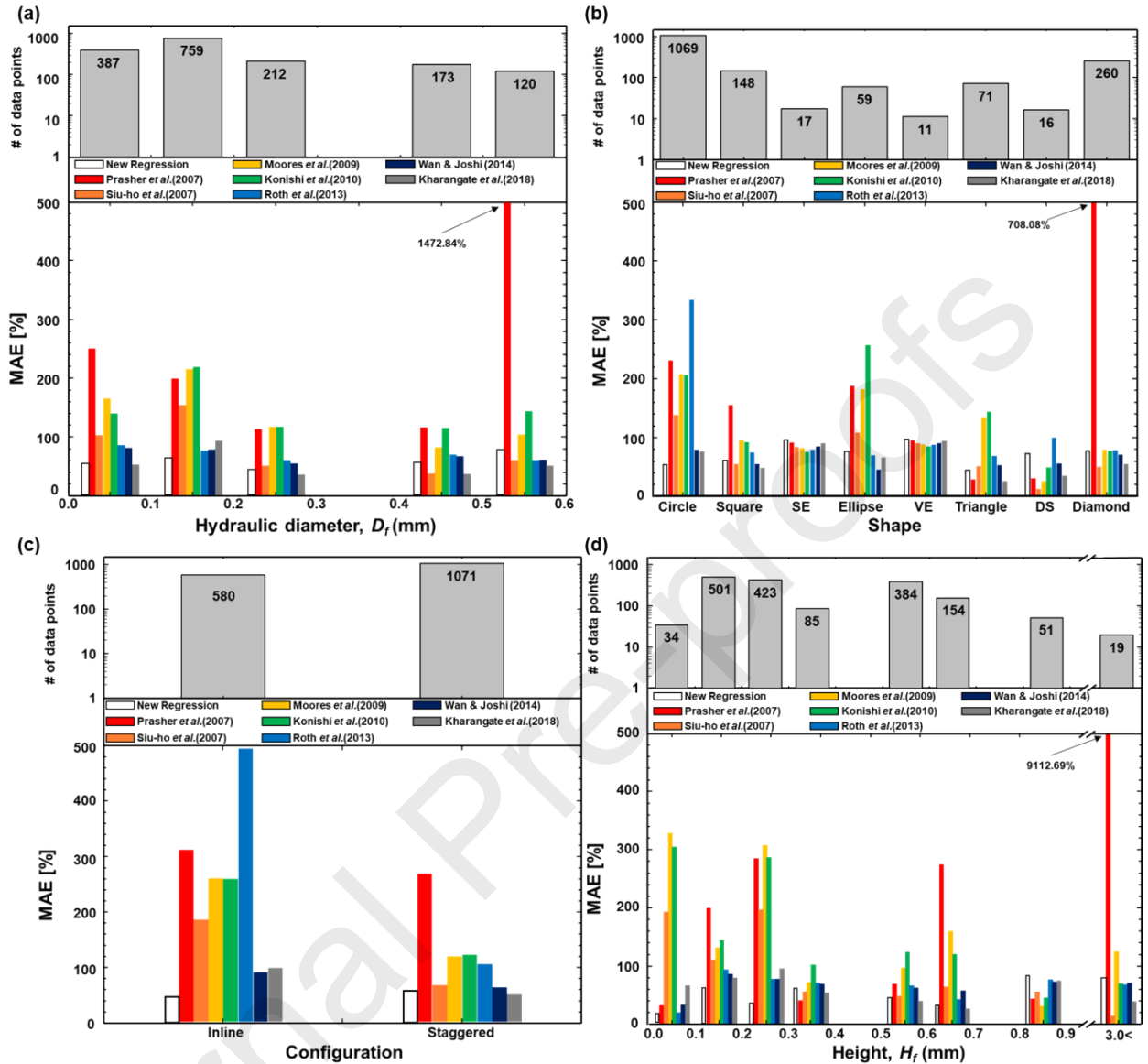
Figure 10 Distribution of MAE in predictions of new regression correlation and previous correlations for data point relative geometrical conditions: (a) hydraulic diameter of pin fin, (b) fin shape, (c) fin configuration, and (d) fin height.

range of f = 0.2–1.0. The larger MAEs in the high f range is because these data points are based on a low flow-rate range, which has relatively high uncertainties. **Figure 9**(b) shows the MAEs according to the Reynolds number. Since the data with Reynolds number between 0 and 300 occupies 68.20% of the total data points, it can be expected that this range of data has a greater impact on the results than other ranges of data. Therefore, the present regression correlation provides the best predictions in the range of Re < 1200 but relatively high MAEs (> 200%) in the higher Re range (Re > 1200), since data points are insufficient. Wan & Joshi [19] has also provided good predictions in the low Re range because this was established with experimental data in the

-- 19 --

relatively narrow range of Reynolds number, Re = 22–357. Roth correlation [47] has shown excellent predictions for most f range, but the overall prediction is slightly large due to relatively poor predictions in $f < 0.2$. **Figure 9**(c) illustrates the distribution of MAEs in predictions relative to working fluid. The consolidated database consisted of 85.4% of data points from water; therefore, the present regression correlation exhibits the lowest MAE for water. Most other correlations failed to accurately predict the data in R245fa except for the correlations, such as the new regression correlation, Wan & Joshi [19], and Kharangate *et al.* [20].

Figure 10 illustrates the MAEs according to geometrical parameters of hydraulic diameter, pin fin shape, flow configuration, and fin height. **Figure 10(a)** shows the MAE of each correlation according to the hydraulic diameter (D_f) range of the pin fin. Wan & Joshi [19] and Siu-ho *et al.* [16] correlations have been developed at a fixed fin diameter of D_f = 0.2 mm, but they provide good predictions for $D_f > 0.2$ mm while having slightly higher MAEs in $D_f < 0.2$. The Kharangate correlation [20] has also been developed based on $D_f \sim 0.047$ mm, but it provides evenly good predictions for the whole D_f range. Prasher *et al.* [13], which is based on HDR = 1.3–2.8 with D_f = 0.055–0.153 mm, predicts extremely poorly (MAE = 1472.84%) in $D_f > 0.5$ mm due to large deviations in some data points from Liu *et al.* [31] that have very high aspect ratio ($HDR > 5$).

Figure 10(b) shows the comparison of predictions for different pin fin shapes. As can be seen from the number of data, most data points (89.46%) are experimental results using circle, square, or diamond fin shapes. Therefore, the new correlation has shown a very good prediction for these fin shapes, with fair predictions for other shapes. Since the Siu-Ho correlation [16] has been developed at a square shape where the vortex is likely to occur, the results with square and diamond shapes are superior to shapes such as circle and ellipse. The Konishi correlation [17] especially provides the best prediction for the Ellipse case, while it has been developed using square shape. Additionally, in the new correlation, Wan & Joshi [19] and Kharangate [20] have shown that the differences in MAE are not large and show evenly good predictions for all types of fin shape. **Figure 10(c)** shows the MAE according to the pin fin configuration. Overall, predictions are better for staggered configurations than inline, due to the larger number of data points in staggered fin configurations. In the case of Roth [47], it was developed through experiments on both inline and staggered configurations, but MAE in the inline case is more than four times that in the staggered one. The new correlation shows evenly good predictions, evidenced by MAEs of 45.7% and 55.9% for inline and staggered, respectively. **Figure 10(d)** shows the MAE according to the fin height. The highest MAE, of 9112.69%, was obtained by the Prasher correlation [15] due to the aforementioned reason of the data points with an exceptionally high aspect ratio of $HDR > 5$. The new regression correlation and Roth correlation [47] have shown good predictions at small fin height, of H_f = 0–0.1 mm, since these are only correlations developed using data points with small channel heights of $H_f < 0.1$ mm. In the case of the Siu-Ho [16], Moores [45], and

Konishi [17] correlations, the MAEs at $H_f < 0.1$ mm are high since these correlations are based on heights of 0.67 mm, 0.2–0.4 mm, and 0.67 mm, respectively.

3.2 Assessment of the new ANN model

Figure 11 shows the prediction of our MLP model for the consolidated database. **Figure 11(a)** shows the overall predictive accuracy for all consolidated data points, while **Figure 11(b)** is only for data points in the test set to validate the predictive accuracy for unseen data. As shown in this figure, the prediction by our MLP model shows an incredibly improved MAE of 11.88% compared to correlations by regression models, which have the lowest MAE of 52.33%. Moreover, our MLP model has much better-predicting capabilities for wide geometrical and operational ranges, evidenced by $\theta = 90.67\%$ and $\xi = 96.55\%$ percentage of data points predicted within ±30% and ±50%. The good predicting accuracy is still preserved for unseen data points, as shown in **Figure 11(b)** with MAE of 14.49%, $\theta = 85.54\%$, and $\xi = 92.77\%$.
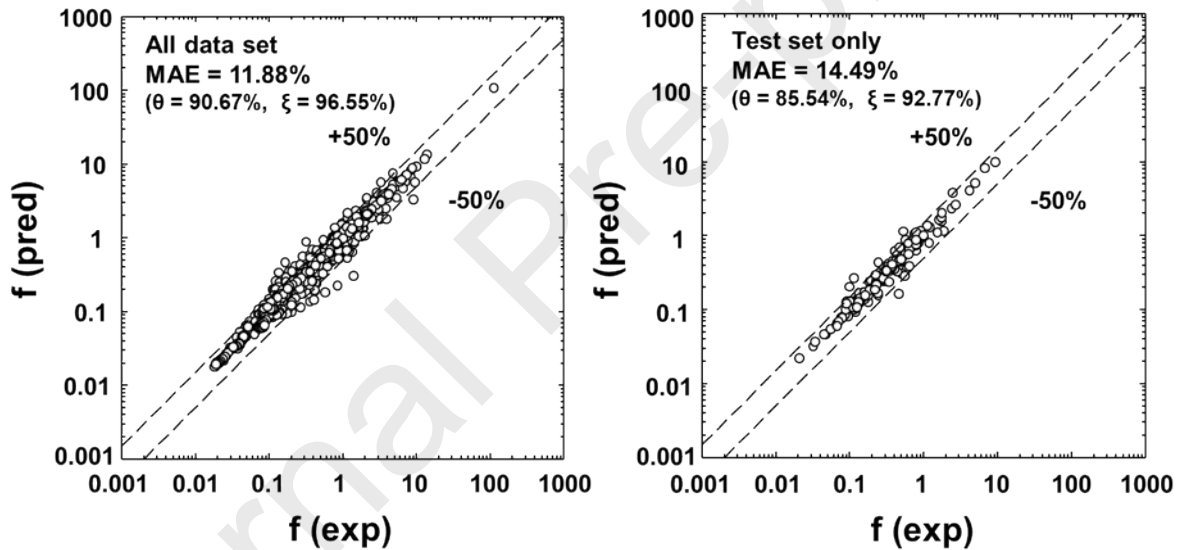
Figure 11 Comparison of experimentally determined Fanning friction factor with predictions of the MLP model for a) all data set and b) for test data sets.

Figure 12 shows the comparison of predictive accuracy by the new regression correlation and ANN model according to operating conditions of f, Re, and working fluid. MAEs are significantly reduced using our MLP model for all f and Re ranges and types of a working fluid. In **Figure 12**(a), our MLP model shows the largest MAE in f between 0.4 to 0.5 with an MAE of 13.54%, but in all ranges, there is an MAE of 8.5–13.7% with a small deviation. The regression correlation provides relatively bad predictions for a larger f range of $f > 0.7$, but the MLP does not show a significant difference depending on different f ranges.
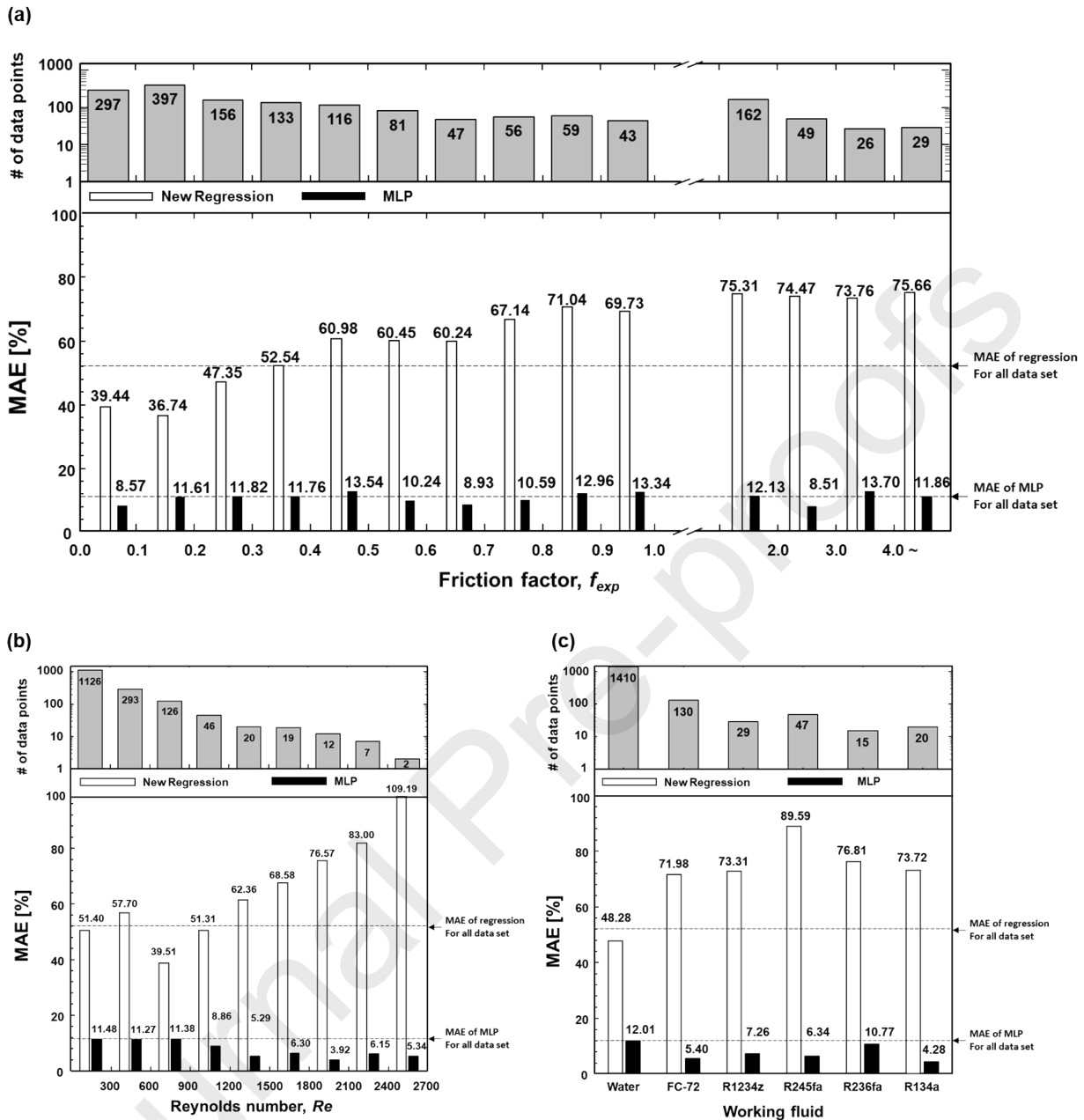
Figure 12 Distribution of MAE in predictions of new regression correlation and MLP model according to operational conditions: (a) friction factor, (b) Reynolds number, and (c) working fluid.

Figure 12(b) shows the distribution of MAE, according to *Re*. The highest MAE is found in the 0-300 range, but MAE is still low at 11.5%. The range of *Re* > 900 gives lower MAE, of 3–9%, than those from *Re* < 900, which is probably caused by the high uncertainty in low *Re* range from low flow rates. **Figure 12**(c) shows the MAE distribution for working fluid. Our MLP model provides evenly good predictions for all working fluids, while the regression model shows large MAE differences for types of a working fluid. Our MLP model shows the highest MAE of 12.01%

-- 22 --

for water, while the regression correlation shows the lowest MAE for water, 48.28%, since 85% of the consolidated data (1,410 data points) have water as the working fluid. The biggest cause of the high MAE with water in the MLP model is from underpredicted f in square and triangle shapes due to the characteristic of the shapes causing a higher pressure drop.

Figure 13 shows the comparison of MAEs for both the new regression model and our MLP model according to geometric parameters of D_f, fin shape, fin configuration, and H_f. **Figure 13**(a) shows the highest MAE, of 21.59%, for D_f = 0.2–0.3 mm, while MAE = 5.49–15.39% for other hydraulic diameter ranges. The data in D_f = 0.2–0.3 mm has high MAE, mainly due to data points from Zhao *et al.*[36] Siu-ho *et al.* [16], and Guan *et al.*[38], which have MAEs > 40%.

Figure 13(b) shows the MAE distribution for different fin shapes. Our MLP model shows relatively high MAEs for square and triangle fin shapes. Zhao *et al.* [36] and Guan *et al.* [38] claimed that square and triangle tend to show lower f at laminar and higher at turbulent than round shapes like circle or ellipse due to the eddy effect at turbulent, resulting in the underprediction of f for these shapes. **Figure 13**(c, d) shows the MAE distribution with fin height and flow configuration. Our MLP model shows the highest MAE, 17.34%, at H_f = 0.5–0.6 mm, since many data points in this height range are square and triangle fin shapes. Similarly, the staggered flow configuration has a higher MAE of 12.49% than that for the inline of MAE = 8.65% due to the same reason.

Figure 14 shows the MAE comparison of the new regression correlation and our MLP model against the individual Fanning friction databases from 22 sources. Our MLP model provides evenly good predictions, evidenced by a range of MAE,2.63–18.52%, except for high MAEs of 36.22% and 22.79% for Siu-ho *et al.* [16] and Zhao *et al.* [36], respectively. The prediction for Siu-ho *et al.* [16] data shows the highest MAE and is even higher than that by the new regression model. This result comes from different predicting accuracy with respect to pin fin shape and Reynolds number for the new regression and ANN model. Siu-Ho *et al.* data consist of Re = 0–700 with square fin shape, where the regression model shows fair prediction accuracies compared to others. However, the predictions for square fin shape within Re = 0–900 are especially poor in the ANN model compared to those Re > 900, as shown in **Fig. 12.** Zhao *et al.* [36] experimented with various shapes. Among them, the results of experiments with diamonds and triangle shapes showed high MAEs of 36.32% and 31.52%, respectively, while it showed relatively good predictions of MAE of 12.69% for ellipse, 18.84% for circle, and 18.51% for square. The detailed predictive accuracies are summarized in **Table S2** in the supplementary information.
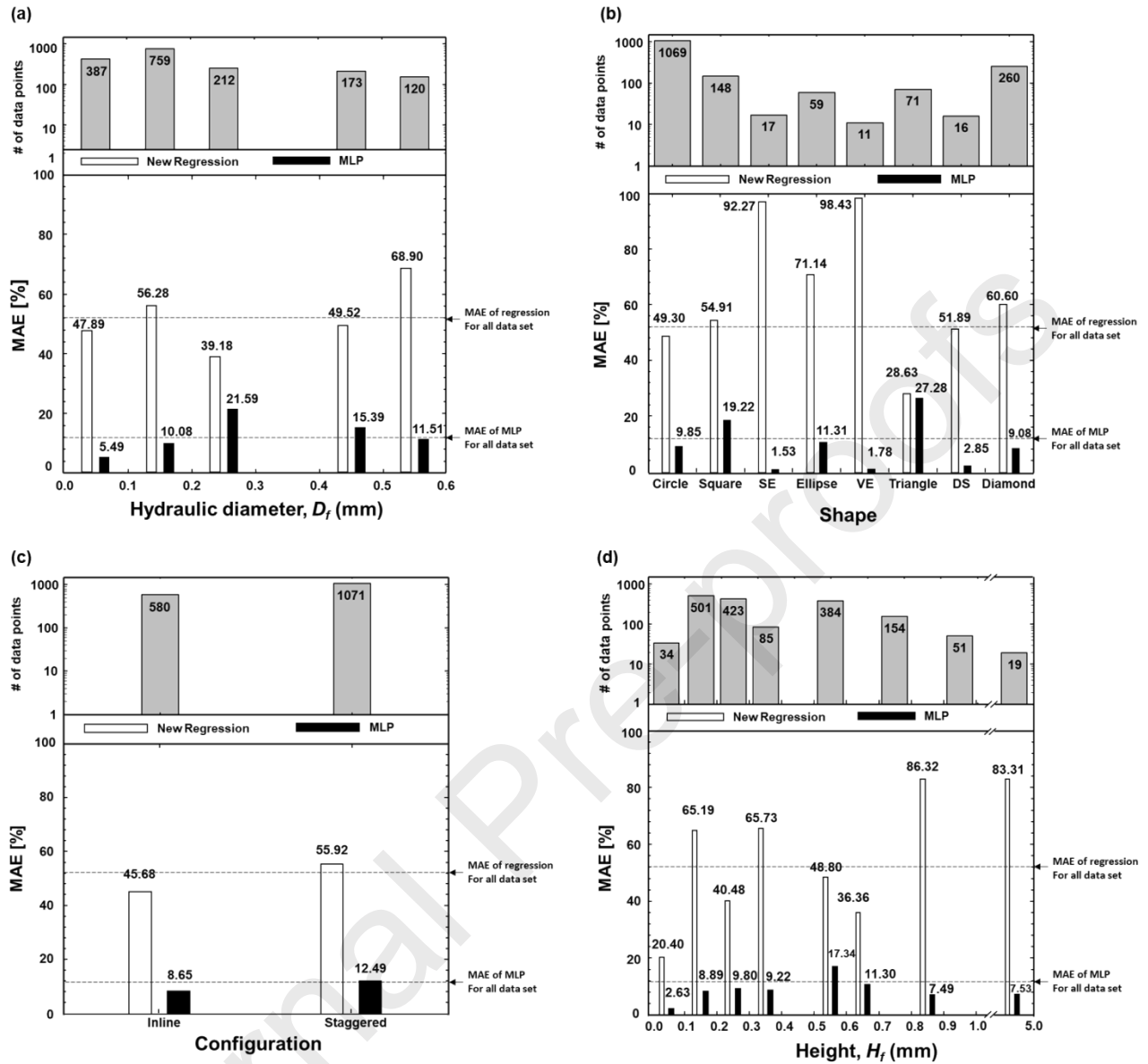
Figure 13 Distribution of MAE in predictions of MLP for data point relative geometrical conditions: (a) Hydraulic diameter of pin fin, (b) fin shape, (c) fin configuration, and (d) height.
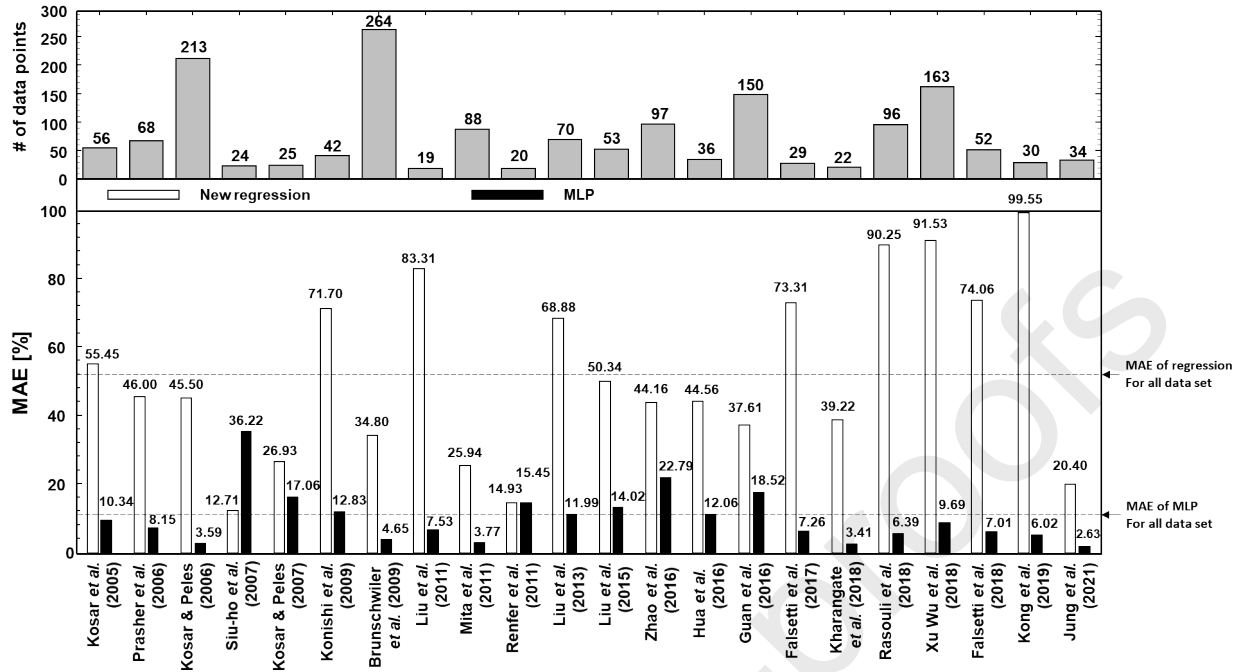
Figure 14 Comparison of individual experimentally determined friction factor data points with MLP.

4. Conclusions

This study is part of two studies conducted to develop artificial-neural-network-based tools for predicting the pressure drop and heat transfer coefficient in micro-pin fin heat sinks with various geometries for various operational ranges, to overcome the limitations of conventional regression models. In this study, we adopted a universal approach to predict the frictional pressure drop for flows in micro-pin fin arrays. Universal models were developed on the basis of a consolidated database amassed from 22 published studies. The consolidated database comprised 1,651 frictional pressure drop data points for six different working fluids, eight different fin shapes, and Reynolds numbers (*Re*) in the range 0–2500. Two different universal approaches were examined: using i) conventional regression method and ii) multilayer perceptron (MLP) neural network. Prediction accuracies of the developed universal models were compared with those of previous relevant correlations. We categorized seven relevant correlations into two groups, with one group containing correlations without any geometric term and the other containing correlations with at least one geometric term. The key results of the study are as follows:

    (1) In the first group (containing correlations without any geometric term), Kharangate *et al.*'s [20] correlation showed the best prediction (MAE = 68.43%), while in the other group, the new correlation based on the conventional regression method provided the most accurate result (MAE = 52.33%).

-- 25 --

(2) A new MLP, a type of artificial neural network, with 12 hidden layers and 28 nodes for each layer was developed, and the prediction accuracies were compared with those of relevant correlations for a wide range of geometric and operating parameters namely the friction factor, Reynolds number, type of the working fluid, fin hydraulic diameter, fin shape, fin height, and flow configuration. Overall, our MLP model showed superior prediction accuracy for almost every condition, and its MAE was 11.88% for all data and 14.49% for the test data set, indicating almost fivefold enhancements. Furthermore, 90.67% of the total data was predicted within the 30% error range and 96.55% of the total data was within the 50% error range.

(3) The MAE of MLP predictions was relatively small for some geometries with sharpened shapes such as square and triangle, due to missing parameters to quantify the sharpened shape, but further improvement can be expected if detailed fin shape can be trained during neural network modeling.

(4) A neural network is a group of interconnected artificial neurons; it processes information based on a connectionist approach to computation. Therefore, if it does not overfit, it outperforms the existing regression method. Because the proposed method determines the friction factor correlation with a neural network method based on various literature sources, the approach can be used as a general-purpose prediction method for micro-pin fins with different spacing and operating conditions.

References

[1] W. Qu, I. Mudawar, Experimental and numerical study of pressure drop and heat transfer in a single-phase micro-channel heat sink, Int. J. Heat Mass Transf. 45 (2002) 2549–2565. https://doi.org/10.1016/S0017-9310(01)00337-4.

[2] A. Husain, K.Y. Kim, Design optimization of manifold microchannel heat sink through evolutionary algorithm coupled with surrogate model, IEEE Trans. Compon. Packag. Manuf. Technol. 3 (2013) 617–624. https://doi.org/10.1109/TCPMT.2013.2245943.

[3] J. Kim, Spray cooling heat transfer: The state of the art, Int. J. Heat Fluid Flow. 28 (2007) 753−767. https://doi.org/10.1016/j.ijheatfluidflow.2006.09.003.

[4]   D. Lytle, B.W. Webb, Air jet impingement heat transfer at low nozzle-plate spacings, Int. J. Heat Mass Transf. 37 (1994) 1687–1697. https://doi.org/10.1016/0017-9310(94)90059-0.

[5]   W. Escher, T. Brunschwiler, B. Michel, D. Poulikakos, Experimental investigation of an ultrathin manifold microchannel heat sink for liquid-cooled chips, J. Heat Transfer. 132 (2010) 1–10. https://doi.org/10.1115/1.4001306.

[6]   G.P. Peterson, A.B. Duncan, M.H. Weichold, Experimental investigation of micro heat pipes fabricated in silicon wafers, J. Heat Transfer. 115 (1993) 751–756. https://doi.org/10.1115/1.2910747.

[7]   S. Launay, V. Sartre, M. Lallemand, Experimental study on silicon micro-heat pipe arrays, Appl. Therm. Eng. 24 (2004) 233–243. https://doi.org/10.1016/j.applthermaleng.2003.08.003.

[8]   R. Chen, M.C. Lu, V. Srinivasan, Z. Wang, H.H. Cho, A. Majumdar, Nanowires for enhanced boiling heat transfer, Nano Lett. 9 (2009) 548–553. https://doi.org/10.1021/nl8026857.

[9]   J.M. Koo, S. Im, L. Jiang, K.E. Goodson, Integrated microchannel cooling for three-dimensional electronic circuit architectures, J. Heat Transfer. 127 (2005) 49–58. https://doi.org/10.1115/1.1839582.

[10]   D. Sekar, C. King, B. Dang, T. Spencer, H. Thacker, P. Joseph, M. Bakir, J. Meindl, A 3D-IC technology with integrated microchannel cooling, in: 2008 International Interconnect Technology Conference, IEEE, Burlingame, CA, USA, 2008: pp. 13–15. https://doi.org/10.1109/IITC.2008.4546911.

[11]   X. Zhang, X. Han, T.E. Sarvey, C.E. Green, P.A. Kottke, A.G. Fedorov, Y. Joshi, M.S. Bakir, Three-dimensional integrated circuit with embedded microfluidic cooling: Technology, thermal performance, and electrical implications, J. Electronic Packaging. 138 (2016) 010910. https://doi.org/10.1115/1.4032496.

[12]   A. Koşar, C. Mishra, Y. Peles, Laminar flow across a bank of low aspect ratio micro pin fins, J. Fluids Eng. Trans. ASME. 127 (2005) 419–430. https://doi.org/10.1115/1.1900139.

[13]   A. Kosar, Y. Peles, Micro scale pin fin heat sinks — Parametric performance evaluation study, IEEE Trans. Compon. Packag. Manuf. Technol. 30 (2007) 855–865 http://doi.org/10.1109/TCAPT.2007.906334

[14]   A. Koşar, Y. Peles, Thermal-hydraulic performance of MEMS-based pin fin heat sink, J. Heat Transfer. 128 (2006) 121–131. https://doi.org/10.1115/1.2137760.

[15]   R.S. Prasher, J. Dirner, J.Y. Chang, A. Myers, D. Chau, D. He, S. Prstic, Nusselt number and friction factor of staggered arrays of low aspect ratio micropin-fins under cross flow for water as fluid, J. Heat Transfer. 129 (2007) 141–153. https://doi.org/10.1115/1.2402179.

[16] A. Siu-Ho, W. Qu, F. Pfefferkorn, Experimental study of pressure drop and heat transfer in a single-phase micropin-fin heat sink, J. Electron. Packag. 129 (2007) 479–487. https://doi.org/10.1115/1.2804099.

[17] C.A. Konishi, W. Qu, F.E. Pfefferkorn, Experimental study of water liquid-vapor two-phase pressure drop across an array of staggered micropin-fins, J. Electron. Packag. Trans. ASME. 131 (2009) 0210101–0210108. https://doi.org/10.1115/1.3104028.

[18] J.F. Tullius, T.K. Tullius, Y. Bayazitoglu, Optimization of short micro pin fins in minichannels, Int. J. Heat Mass Transf. 55 (2012) 3921–3932. https://doi.org/10.1016/j.ijheatmasstransfer.2012.03.022.

[19] Z. Wan, Y. Joshi, Pressure drop and heat transfer characteristics of pin fin enhanced microgaps in single phase microfluidic cooling, Int. J. Heat Mass Transf. 115 (2017) 115–126. https://doi.org/10.1016/j.ijheatmasstransfer.2017.06.117.

[20] C.R. Kharangate, K.W. Jung, S. Jung, D. Kong, J. Schaadt, M. Iyengar, C. Malone, H. Lee, M. Asheghi, K.E. Goodson, Experimental investigation of embedded micropin-fins for single-phase heat transfer and pressure drop, J. Electron. Packag. Trans. ASME. 140 (2018). https://doi.org/10.1115/1.4039475.

[21] D. Kong, K.W. Jung, S. Jung, D. Jung, J. Schaadt, M. Iyengar, C. Malone, C.R. Kharangate, M. Asheghi, K.E. Goodson, H. Lee, Single-phase thermal and hydraulic performance of embedded silicon micro-pin fin heat sinks using R245fa, Int. J. Heat Mass Transf. 141 (2019) 145–155. https://doi.org/10.1016/j.ijheatmasstransfer.2019.05.073.

[22] K.A. Moores, Y.K. Joshi, Effect of tip clearance on the thermal and hydrodynamic performance of a shrouded pin fin array, J. Heat Transfer. 125 (2003) 999–1006. https://doi.org/10.1115/1.1621897.

[23] D. Mei, X. Lou, M. Qian, Z. Yao, L. Liang, Z. Chen, Effect of tip clearance on the heat transfer and pressure drop performance in the micro-reactor with micro-pin-fin arrays at low Reynolds number, Int. J. Heat Mass Transf. 70 (2014) 709–718. https://doi.org/10.1016/j.ijheatmasstransfer.2013.11.060.

[24] M.K. Chyu, Heat transfer and pressure drop for short pin-fin arrays with pin-endwall fillet, J. Heat Transfer. 112 (1990) 926–932. https://doi.org/10.1115/1.2910502.

[25] T.-M. Jeng, S.-C. Tzeng, Pressure drop and heat transfer of square pin-fin arrays in in-line and staggered arrangements, Int. J. Heat Mass Transf. 50 (2007) 2364–2375. https://doi.org/https://doi.org/10.1016/j.ijheatmasstransfer.2006.10.028.

[26] C. Woodcock, F. Houshmand, J. Plawsky, M. Izenson, D. Fogg, R. Hill, S. Phillips, Y. Peles, Piranha Pin-Fins (PPF): Voracious boiling heat transfer by vapor venting from microchannels -System calibration and single-phase fluid dynamics, Thermomechanical

Phenom. Electron. Syst. -Proceedings Intersoc. Conf. (2014) 282–289. https://doi.org/10.1109/ITHERM.2014.6892294.

[27] T.E. Sarvey, Y. Hu, C.E. Green, P.A. Kottke, D.C. Woodrum, Y.K. Joshi, A.G. Fedorov, S.K. Sitaraman, M.S. Bakir, Integrated circuit cooling using heterogeneous micropin-fin arrays for nonuniform power maps, IEEE Trans. Components, Packag. Manuf. Technol. 7 (2017) 1465–1475. https://doi.org/10.1109/TCPMT.2017.2704525.

[28] Y.-J. Lee, P.-S. Lee, S.-K. Chou, Enhanced microchannel heat sinks using oblique fins, (2009) 253–260. https://doi.org/10.1115/InterPACK2009-89059.

[29] Z. Liu, C. Zhang, H. Zhao, N. Guan, Forced convective heat transfer characteristics in micro/minicylinders group at low Reynolds number, nanoscale microscale thermophys. Eng. 16 (2012) 165–180. https://doi.org/10.1080/15567265.2012.683933.

[30] T. Brunschwiler, B. Michel, H. Rothuizen, U. Kloter, B. Wunderle, H. Oppermann, H. Reichl, Interlayer cooling potential in vertically integrated packages, Microsyst. Technol. 15 (2009) 57–74. https://doi.org/10.1007/s00542-008-0690-4.

[31] M. Liu, D. Liu, S. Xu, Y. Chen, Experimental study on liquid flow and heat transfer in micro square pin fin heat sink, Int. J. Heat Mass Transf. 54 (2011) 5602–5611. https://doi.org/10.1016/j.ijheatmasstransfer.2011.07.013.

[32] J.R. Mita, W. Qu, M.H. Kobayashi, F.E. Pfefferkorn, Experimental study and numerical analysis of water single-phase pressure drop across an array of circular micro-pin–fins, in: Proceedings of ASME/JSME AJTEC2011-44583, Honolulu, Hawaii, USA, 2011 https://doi.org/10.1115/AJTEC2011-44583

[33] A. Renfer, M.K. Tiwari, T. Brunschwiler, B. Michel, D. Poulikakos, Experimental investigation into vortex structure and pressure drop across microcavities in 3D integrated electronics, Exp. Fluids. 51 (2011) 731–741. https://doi.org/10.1007/s00348-011-1091-5.

[34] Z. Liu, Z. Wang, C. Zhang, N. Guan, G. Jiang, Flow resistance and heat transfer characteristics in micro-cylinders-group, Heat Mass Transf. Und Stoffueebertragung. 49 (2013) 733–744. https://doi.org/10.1007/s00231-013-1115-1.

[35] Z.G. Liu, N. Guan, C.W. Zhang, G.L. Jiang, The Flow Resistance and Heat Transfer Characteristics of Micro Pin-Fins with Different Cross-Sectional Shapes, Nanoscale Microscale Thermophys. Eng. 19 (2015) 221–243. https://doi.org/10.1080/15567265.2015.1073820.

[36] H. Zhao, Z. Liu, C. Zhang, N. Guan, H. Zhao, Pressure drop and friction factor of a rectangular channel with staggered mini pin fins of different shapes, Exp. Therm. Fluid Sci. 71 (2016) 57–69. https://doi.org/10.1016/j.expthermflusci.2015.10.010.

[37] J. Hua, G. Li, X. Zhao, Q. Li, J. Hu, Study on the flow resistance performance of fluid cross various shapes of micro-scale pin fin, Appl. Therm. Eng. 107 (2016) 768–775. https://doi.org/10.1016/j.applthermaleng.2016.07.048.

[38] N. Guan, T. Luan, G. Jiang, Z.G. Liu, C.W. Zhang, Influence of heating load on heat transfer characteristics in micro-pin-fin arrays, Heat Mass Transf. Und Stoffuebertragung. 52 (2016) 393–405. https://doi.org/10.1007/s00231-015-1565-8.C.

[39] Falsetti, M. Magnini, J.R. Thome, Flow boiling heat transfer and pressure drops of R1234ze(E) in a silicon micro-pin fin evaporator, J. Electron. Packag. Trans. ASME. 139 (2017). https://doi.org/10.1115/1.4037152.

[40] E. Rasouli, C. Naderi, V. Narayanan, Pitch and aspect ratio effects on single-phase heat transfer through microscale pin fin heat sinks, Int. J. Heat Mass Transf. 118 (2018) 416–428. https://doi.org/10.1016/j.ijheatmasstransfer.2017.10.105.

[41] F. Xu, H. Wu, Experimental Study of Water Flow and Heat transfer in silicon micro-pin-fin heat sinks, J. Heat Transfer. 140 (2018) 1–13. https://doi.org/10.1115/1.4040956.

[42] C. Falsetti, M. Magnini, J.R. Thome, Hydrodynamic and thermal analysis of a micro-pin fin evaporator for on-chip two-phase cooling of high density power micro-electronics, Appl. Therm. Eng. 130 (2018) 1425–1439. https://doi.org/10.1016/j.applthermaleng.2017.10.117.

[43] D. Jung, H. Lee, D. Kong, E. Cho, K.W. Jung, C. R. Kharangate, M. Iyengar, C. Malone, M. Asheghi, K. E. Goodson, H. Lee, Thermal design and management of micro-pin fin heat sinks for energy-efficient three-dimensional stacked integrated circuits, Int. J. Heat Mass Transfer (in print).

[44] A. Žukauskas, Heat Transfer from Tubes in Crossflow, in: J.P. Hartnett, T.F. Irvine (Eds.), Advances in Heat Transfer, Elsevier, 1972: pp. 93–160. https://doi.org/10.1016/S0065-2717(08)70038-8.

[45] C.L. Hui, S.F. ng, Predicting seam performance of commercial woven fabrics using multiple logarithm regression and artificial neural networks, Text. Res. J. 79 (2009) 1649–1657. https://doi.org/10.1177/0040517509104758.

[46] K.A. Moores, J. Kim, Y.K. Joshi, Heat transfer and fluid flow in shrouded pin fin arrays with and without tip clearance, Int. J. Heat Mass Transf. 52 (2009) 5978–5989. https://doi.org/10.1016/j.ijheatmasstransfer.2009.08.005.

[47] R. Roth, G. Lenk, K. Cobry, P. Woias, Heat transfer in freestanding microchannels with in-line and staggered pin fin structures with clearance, Int. J. Heat Mass Transf. 67 (2013) 1–15. https://doi.org/10.1016/j.ijheatmasstransfer.2013.07.097.

[48] M. Olson, A. Wyner, R. Berk, Modern Neural Networks Generalize on Small Data Sets, in: S. Bengio, H. Wallach, H. Larochelle, K. Grauman, N. Cesa-Bianchi, R. Garnett (Eds.),

Advances in Neural Information Processing Systems 31, Curran Associates, Inc., 2018: pp. 3619–3628.

[49] A.L. Maas, A.Y. Hannun, A.Y. Ng, Rectifier nonlinearities improve neural network acoustic models, ICML Work. Deep Learn. Audio, Speech Lang. Process. 28 (2013).

[50] M.J. Brown, L.A. Hutchinson, M.J. Rainbow, K.J. Deluzio, A.R. De Asha, A comparison of self-selected walking speeds and walking speed variability when data are collected during repeated discrete trials and during continuous walking, J. Appl. Biomech. 33 (2017) 384–387. https://doi.org/10.1123/jab.2016-0355.

[51] K. He, X. Zhang, S. Ren, J. Sun, Delving deep into rectifiers: Surpassing human-level performance on imagenet classification, Proc. IEEE Int. Conf. Comput. Vis. 2015 International Conference on Computer Vision, ICCV 2015 (2015) 1026–1034. https://doi.org/10.1109/ICCV.2015.123.

[52] D.P. Kingma, J.L. Ba, Adam: A method for stochastic optimization, 3rd Int. Conf. Learn. Represent. ICLR 2015 - Conf. Track Proc. (2015) 1–15.J.

[53] J.C. Duchi, P.L. Bartlett, M.J. Wainwright, Randomized smoothing for (parallel) stochastic optimization, Proc. IEEE Conf. Decis. Control. 12 (2012) 5442–5444. https://doi.org/10.1109/CDC.2012.6426698.

[54] T. Tieleman, and G. Hinton, Lecture 6.5 - RMSProp, COURSERA: Neural Networks for Machine Learning.Technical report, (2012).

[55] T. Fushiki, Estimation of prediction error by using K-fold cross-validation, Stat. Comput. 21 (2011) 137–146. https://doi.org/10.1007/s11222-009-9153-8.

[56] U.M. Braga-Neto, E.R. Dougherty, Is cross-validation valid for small-sample microarray classification?, Bioinformatics. 20 (2004) 374–380. https://doi.org/10.1093/bioinformatics/btg419.

[57] G.A. Gabriele, K.M. Ragsdell, The generalized reduced gradient method: A reliable tool for optimal design, J. Manuf. Sci. Eng. Trans. ASME. 99 (1977) 394–400. https://doi.org/10.1115/1.3439249.

[58] L.S. Lasdon, A.D. Waren, A. Jain, M. Ratner, Design and testing of a generalized reduced gradient code for nonlinear programming, ACM Trans. Math. Softw. 4 (1978) 34–50. https://doi.org/10.1145/355769.355773.

Supplementary Information

Appendix A. Selection of numbers of hidden layers and nodes

Table S1 MAE of different combinations of layers and nodes.

Layer Node	4 layers		8 layers		12 layers		16 layers	
	training	validation	training	validation	training	validation	training	validation
4	103.83	75.22	143.00	100	39.69	29.26	71.83	57.56
8	42.75	34.58	30.00	19.85	22.44	20.09	149.75	76.04
12	54.32	56.62	25.14	21.48	27.34	19.70	57.36	63.61
16	83.02	85.85	31.70	12.45	30.47	18.09	27.84	27.96
20	42.34	36.71	105.66	15.06	46.25	13.68	159.54	73.31
24	33.37	37.07	75.88	51.85	54.53	12.81	38.84	38.83
28	55.12	65.01	97.67	71.18	12.31	13.01	17.31	18.77
32	52.44	58.88	26.22	30.55	37.05	11.41	32.30	35.39
36	38.78	34.89	45.97	57.53	71.13	12.21	98.15	52.07
40	37.14	40.15	39.22	37.46	17.34	15.44	41.41	38.04

Table S1 shows a combination of four kinds of layers and 10 kinds of nodes. In this study, three combination sets of layers and nodes that have lower than 20% of both train MAE and validation MAE were chosen: 12layer 28node, 16layer 28node, and 12layer 40node. 12layer 28node were chosen because it shows the minimum difference between train MAE and validation MAE. This means model is not over- or under-fitted. 12layer 28node also shows the lowest validation MAE among the three sets.

Appendix B. Comparison θ and ξ of new regression and ANN mode for each individual study

Table S2 θ and ξ of regression and MLP by each paper

Author	Total data points	Regression θ [%]	Regression ξ [%]	MLP θ [%]	MLP ξ [%]
Koşar *et al.* (2005)	56	32.14	44.64	96.43	98.21
Prasher *et al.* (2006)	68	22.06	38.24	94.12	98.53
Kosar & Peles (2006)	213	33.33	50.23	79.25	91.51
Siu-Ho *et al.* (2007)	24	100.00	100.00	66.67	75
Kosar & Peles (2007)	25	68.00	96.00	100.00	100.00
Konishi *et al.* (2009)	42	0.00	0.00	78.57	92.86
Brunschwiler *et al.* (2009)	264	37.50	60.98	99.24	99.62

Liu *et al.* (2011)	19	47.37	73.68	89.47	94.74
Mita & Qu (2011)	88	43.18	89.77	100.00	100.00
Renfer *et al.* (2011)	20	30.00	75.00	100.00	100.00
Liu *et al.* (2013)	70	0.00	5.71	95.71	100.00
Liu *et al.* (2015)	53	0.00	39.62	100.00	100.00
Zhao *et al.* (2016)	97	31.96	71.13	79.38	87.63
Hua *et al.* (2016)	36	36.11	66.67	88.89	97.22
Guan *et al.* (2016)	150	42.00	68.00	86.67	96.67
Falsetti *et al.* (2017)	29	0.00	0.00	96.55	100
Kharangate *et al.* (2018)	22	0.00	100.00	100.00	100.00
Rasouli *et al.* (2018)	96	0.00	0.00	92.71	100.00
Xu Wu *et al.* (2018)	163	0.00	0.00	91.41	99.39
Falsetti *et al.* (2018)	52	0.00	0.00	100.00	100.00
Kong *et al.* (2019)	30	80.00	100.00	96.67	100.00
Jung *et al.* (2021)	34	0.00	0.00	100.00	100.00
All	1651	25.92	45.25	91.46	96.97

Table S2 compares the θ and ξ of regression and MLP by individual experimental study. The prediction by the new regression model is the worst for Siu-Ho *et al.* [16] data of MAE = 12.71% being θ = 95.8%, ξ = 100%, followed by Renfer *et al.* [33] with MAE = 14.93%, θ = 90% and ξ = 95%. Although Kharangate *et al.* [20] data shows θ = 9.1%, all errors are under 50%. In the case of MLP, most papers have a ξ of 90% or more. ξ values of Zhao *et al.* [36] and Siu-Ho *et al.* [16] is lower than 90%. In the case of Zhao *et al.* [36], MAE is high when the shape is square, diamond, or triangle, while Siu-Ho *et al.* [16] conducted with a square fin shape.

Table 3 Summary of frictional friction factor studies for micro-pin fins included in the consolidated database.

...pe	Config	Fluid	f	Re	D_f [mm]	H_f [mm]	q'' [W/cm²]	Operating condition	Total data points	Included data points	...
D	ST IN	Water	0.27 - 8.25	5 – 100	0.05 - 0.1	0.1 – 0.2	Adiabatic	$\dot{m}$ = 0.47 – 3.9 g/min, T_{in} = 22 ºC	56	56	Converting from
S	ST	Water	0.09 - 1.14	40 – 1000	0.055 - 0.15	0.2 – 0.31	Adiabatic	$\dot{m}$ = 9.98 – 199.6 g/min, ΔP = 0 – 250 kPa, T_{in} = 50 ºC	68	68	
D	ST IN	Water	0.08 - 12.75	3.1 – 271.8	0.035 - 0.1	0.243	Adiabatic		213	213	Converting from
S	ST	Water	0.07 - 0.16	120 – 700	0.2	0.67	50 – 100	T_{in} = 25 ºC, $\dot{m}$ = 83.4 – 644.2 g/min	24	24	
C	ST	Water	0.18 - 2.03	14 – 250	0.1	0.1 – 0.243	Adiabatic	$\dot{m}$ = 0.6 – 9 g/min	59	25	Excluding some
S	ST	Water	0.4 - 0.83	35 – 260	0.2	0.67	Adiabatic	T_{in} = 21 – 80 ºC, $\dot{m}$ = 36.6 – 90.6 g/min	42	42	
DS	ST IN	Water	0.02 - 111.57	<1000	0.025 - 0.1	0.1 – 0.2	Adiabatic	$\dot{m}$ = 50 – 210 g/min, T_{in} = 25 ºC	307	264	Pearl chain sh... e...
D	ST	Water	0.13 - 0.59	80 – 700	0.63 - 0.79	3.0	50 – 350	Q = 5.693 – 57.221 L/h, T_{in} = 30 – 70 ºC	19	19	Converting
C	ST	Water	0.12 - 0.4	25 – 800	0.18	0.683	Adiabatic	T_{in} = 23 – 80 ºC, $\dot{m}$ = 34.32 – 318.9 g/min	88	88	Converting
C	IN	Water	0.07 - 0.58	14.5 – 270.4	0.1	0.2	Adiabatic		20	20	Calculating f
C	ST IN	Water	0.18 - 1.1	8.6 – 396.5	0.5	0.5	Adiabatic		70	70	Converting
E, D	ST	Water	0.06 - 0.85	108.6 – 970.2	0.4 - 0.56	0.5	Adiabatic		53	53	Converting
S, E, T	ST	Water	0.02 - 1.39	100 – 2500	0.28 - 0.72	0.5	Adiabatic		97	97	Converting
C	ST	Water	0.04 - 1.76	70 – 1700	0.4	0.3	Adiabatic	$\dot{m}$ = 0 – 199.6 g/min, ΔP = 0 ~ 40 kPa	36	36	Only new... f from pr...
D, T	ST	Water	0.18 - 1.21	47 – 922.8	0.28 - 0.72	0.5	*50 – 150 W		150	150	Calculating f *Heated a...
C	IN	R1234ze (E)	0.09 - 0.18	230 – 2500	0.05	0.1	20 – 44	T_{out} = 25, 30, 35 ºC	29	29	Converting
C	ST	Water	0.2 -0.5	23 - 135	0.047	0.11	24 – 141.4	$\dot{m}$ = 15.1 – 64.1 g/min, P_{in} = 144.4 ~ 340.1 kPa, P_{out} = 132.0 – 201.0 kPa, T_{in} = 25 ºC, T_{out} = 31.5 – 84.3ºC	22	22	
D	ST	FC-72	0.69 - 5.33	15 - 1500	0.18 - 0.2	0.396 – 0.845	Adiabatic		Not specified	96	Exact numb...
S, E, VE	ST IN	Water	0.27 - 3.96	40 – 1000	0.1 - 0.15	0.11	Adiabatic	$\dot{m}$ = 3 – 42 g/min, T_{in} > 30 ºC	163	163	Converting
C	IN	R236fa, R134a, R245fa	0.1 - 0.31	230 – 2500	0.05	0.1	20 – 44	T_{out} = 25 ºC	52	52	Converting from
C	ST	R245fa	0.03 - 0.51	35 – 500	0.045 - 0.1	0.2 – 0.208	2.5 – 48.7	T_{in} = 22.2 – 25.3 ºC, $\dot{m}$ = 14.7 – 181.6 g/min	30	30	
C	ST	FC-72	0.08 - 0.18	81 – 182	0.038	0.091	0 – 60	Q = 70 – 140 g/min	34	34	

Table 4 Previous micro-pin fin friction factor correlations.

	Author(s)	Equation	Fluid	Geometry
1	Present study	$f = 3.704\left(\dfrac{H_f}{D_f}\right)^{-0.214}\left(\dfrac{S_L - D_f}{D_f}\right)^{0.349}\left(\dfrac{S_T - D_f}{D_f}\right)^{-0.870}\left(\dfrac{D_W}{D_f}\right)^{1.656}\left(\dfrac{D_L}{D_f}\right)^{2.708} \mathrm{Re}^{-0.668}$ for $Re < 100$ $f = 0.270\left(\dfrac{H_f}{D_f}\right)^{0.620}\left(\dfrac{S_L - D_f}{D_f}\right)^{0.710}\left(\dfrac{S_T - D_f}{D_f}\right)^{-0.501}\left(\dfrac{D_W}{D_f}\right)^{0.050}\left(\dfrac{D_L}{D_f}\right)^{0.047} \mathrm{Re}^{-0.294}$ for $Re > 100$ $f = 1.569\left(\dfrac{H_f}{D_f}\right)^{0.244}\left(\dfrac{S_L - D_f}{D_f}\right)^{0.164}\left(\dfrac{S_T - D_f}{D_f}\right)^{-0.919}\left(\dfrac{D_W}{D_f}\right)^{1.851}\left(\dfrac{D_L}{D_f}\right)^{0.367} \mathrm{Re}^{-0.539}$ for all Re	Water FC72 R1234ze R134a R236fa R245fa	Staggered & Circle, Squar Diamond, D: $25\mu m < D_f <$ $H_f = 0.09 - 3$ $S_T = 0.05 - 1$ $S_L = 0.05 - 1$
2	Prasher et al. [15]	$f = 169.82\left(\dfrac{H_f}{D_f}\right)^{-0.640}\left(\dfrac{S_L - D_f}{D_f}\right)^{-0.258}\left(\dfrac{S_T - D_f}{D_f}\right)^{0.283} \mathrm{Re}^{-1.350}$ for $Re < 100$ $f = 0.295\left(\dfrac{H_f}{D_f}\right)^{1.249}\left(\dfrac{S_L - D_f}{D_f}\right)^{-0.700}\left(\dfrac{S_T - D_f}{D_f}\right)^{-0.360} \mathrm{Re}^{-0.100}$ for $Re < 100$	Water	Staggered, C $55\ \mu m < D_f <$ $1.3 < H_f/D_f <$ $2 < S_T/D_f <$ $2 < S_L/D_f <$
3	Siu-ho et al. [16]	$f = 5.023\,\mathrm{Re}^{-0.547}$	Water	Staggered, S $D_f = 200\ \mu m$ $H_f = 670\ \mu m$ $S_T = S_L = 400$
4	Moores et al. [46]	$f = 2.63\left(\dfrac{H_f}{D_f}\right)^{0.289} \mathrm{Re}^{-0.390}$	Water	Staggered, C $0.5 < H_f/D_f <$ $1.3 < S_T/D_f <$ $1.13 < S_L/D_f$
5	Konishi et al. [17]	$f = 2.621\,\mathrm{Re}^{-0.350}$	Water	Staggered, S $D_f = 200\ \mu m$ $1.3 < H/D_f <$ $2 < S_T/D_f < 4$ $2 < S_L/D_f < 4$
6	Roth et al. [47]	$f = 12.919\,\mathrm{Re}^{-0.923}$	Water	Staggered & $H_f = 91.1$ & $S_T = 91.1$ & $C/D_f = 0.56$ t
7	Wan & Joshi [19]	$f = 3.355\left(\dfrac{H_f}{D_f}\right)^{-0.356}\left(\dfrac{S_L - D_f}{D_f}\right)^{-0.791}\left(\dfrac{S_T - D_f}{D_f}\right)^{-0.745} \mathrm{Re}^{-0.525}\dfrac{L}{D_f N_L}$ for $Re < 100$ $f = 0.586\left(\dfrac{H_f}{D_f}\right)^{-0.051}\left(\dfrac{S_L - D_f}{D_f}\right)^{-0.175}\left(\dfrac{S_T - D_f}{D_f}\right)^{-0.249} \mathrm{Re}^{-0.552}\dfrac{L}{D_f N_L}$ for $Re > 100$	Water	Staggered, S $D_f = 200\ \mu m$ $H_f/D_f = 1.5$ $S_T/D_f = 2$ $S_L/D_f = 2$
8	Kharangate et al. [20]	$f = 2.5\,\mathrm{Re}^{-0.520}$	Water	Staggered, C $D_f = 46.5\ \mu m$ $H_f/D_f = 2.37$ $S_T/D_f = 2.15$ $S_L/D_f = 2.15$

Supplementary Information

Appendix A. Selection of numbers of hidden layers and nodes

Table S3 MAE of different combinations of layers and nodes.

Layer / Node	Layer4		Layer8		Layer12		Layer16	
	train	validation	train	validation	train	validation	train	validation
4	103.83	75.22	143.00	100	39.69	29.26	71.83	57.56
8	42.75	34.58	30.00	19.85	22.44	20.09	149.75	76.04
12	54.32	56.62	25.14	21.48	27.34	19.70	57.36	63.61
16	83.02	85.85	31.70	12.45	30.47	18.09	27.84	27.96
20	42.34	36.71	105.66	15.06	46.25	13.68	159.54	73.31
24	33.37	37.07	75.88	51.85	54.53	12.81	38.84	38.83
28	55.12	65.01	97.67	71.18	12.31	13.01	17.31	18.77
32	52.44	58.88	26.22	30.55	37.05	11.41	32.30	35.39
36	38.78	34.89	45.97	57.53	71.13	12.21	98.15	52.07
40	37.14	40.15	39.22	37.46	17.34	15.44	41.41	38.04

Appendix B. Comparison θ and ξ of new regression and ANN mode for each individual study

Table S4 θ and ξ of regression and MLP by each paper

Author	Total data points	Regression θ [%]	Regression ξ [%]	MLP θ [%]	MLP ξ [%]
Koşar *et al.* (2005)	56	32.14	44.64	96.43	98.21
Prasher *et al.* (2006)	68	22.06	38.24	94.12	98.53
Kosar & Peles (2006)	213	33.33	50.23	79.25	91.51
Siu-Ho *et al.* (2007)	24	100.00	100.00	66.67	75
Kosar & Peles (2007)	25	68.00	96.00	100.00	100.00
Konishi *et al.* (2009)	42	0.00	0.00	78.57	92.86
Brunschwiler *et al.* (2009)	264	37.50	60.98	99.24	99.62
Liu *et al.* (2011)	19	47.37	73.68	89.47	94.74
Mita & Qu (2011)	88	43.18	89.77	100.00	100.00
Renfer *et al.* (2011)	20	30.00	75.00	100.00	100.00
Liu *et al.* (2013)	70	0.00	5.71	95.71	100.00
Liu *et al.* (2015)	53	0.00	39.62	100.00	100.00
Zhao *et al.* (2016)	97	31.96	71.13	79.38	87.63
Hua *et al.* (2016)	36	36.11	66.67	88.89	97.22
Guan *et al.* (2016)	150	42.00	68.00	86.67	96.67
Falsetti *et al.* (2017)	29	0.00	0.00	96.55	100
Kharangate *et al.* (2018)	22	0.00	100.00	100.00	100.00
et al. (2018)	96	0.00	0.00	92.71	100.00

Xu Wu *et al.* (2018)	163	0.00	0.00	91.41	99.39
Falsetti *et al.* (2018)	52	0.00	0.00	100.00	100.00
Kong *et al.* (2019)	30	80.00	100.00	96.67	100.00
Jung *et al.* (2021)	34	0.00	0.00	100.00	100.00
All	1651	25.92	45.25	91.46	96.97

An artificial neural network model for predicting frictional pressure drop in micro-pin fin heat sinks

Highlights

- Universal approach for predicting frictional pressure drop in micro-pin fin heat sinks for embedded microfluidic cooling is achieved.

- A consolidated database consisting of 1,651 experimental data points of frictional pressure drop in micro-pin fin heat sinks is created from 22 research sources published over the past two decades.

- A conventional regression method based on generalized reduced gradient nonlinear algorithm provides poor predictive accuracies with MAE over 50%

- A multilayer perceptron neural network model shows superior performance with an overall MAE of 11.9% resulting in a 5-fold enhancement in predicting accuracy.

Declaration of interests

☒ The authors declare that they have no known competing financial interests or personal relationships that could have appeared to influence the work reported in this paper.

☐The authors declare the following financial interests/personal relationships which may be considered as potential competing interests: